ARTICLE

CD4+ follicular regulatory T cells optimize the influenza virus–specific B cell response

Yisi Lu[1], Roy Jiang[1,2], Alec W. Freyn[3], Jiawei Wang[2], Shirin Strohmeier[3], Katlyn Lederer[4], Michela Locci[4], Hongyu Zhao[2,5], Davide Angeletti[6], Kevin C. O'Connor[1,7], Steven H. Kleinstein[1,2,8], Raffael Nachbagauer[3], and Joe Craft[1,9]

CD4+ follicular regulatory T (Tfr) cells control B cell responses through the modulation of follicular helper T (Tfh) cells and germinal center development while suppressing autoreactivity; however, their role in the regulation of productive germinal center B cell responses and humoral memory is incompletely defined. We show that Tfr cells promote antigen-specific germinal center B cell responses upon influenza virus infection. Following viral challenge, we found that Tfr cells are necessary for robust generation of virus-specific, long-lived plasma cells, antibody production against both hemagglutinin (HA) and neuraminidase (NA), the two major influenza virus glycoproteins, and appropriate regulation of the BCR repertoire. To further investigate the functional relevance of Tfr cells during viral challenge, we used a sequential immunization model with repeated exposure of antigenically partially conserved strains of influenza viruses, revealing that Tfr cells promote recall antibody responses against the conserved HA stalk region. Thus, Tfr cells promote antigen-specific B cell responses and are essential for the development of long-term humoral memory.

Introduction

Antibodies form the first line of defense against invading pathogens and provide the basis for many successful vaccines through establishing a humoral memory response (Nutt et al., 2015). One of the hallmarks of humoral immunity is the progressive increase in the affinity of antibodies over time, a process occurring in germinal centers (GCs) within B cell follicles of secondary lymphoid organs (De Silva and Klein, 2015; Eisen, 2014). Upon encounter with pathogens, B cells mature into memory B cells and long-lived antibody-producing plasma cells (LLPCs) in GCs. Following reexposure to the pathogen, high-affinity protective antibodies secreted by LLPCs are a first line of protection; additionally, pathogen-specific memory B cells are activated and rapidly mature into plasmablasts to produce protective antibodies (De Silva and Klein, 2015). Within the GC, B cells undergo proliferation and somatic hypermutation of Ig genes, followed by a process in which the "fittest" B cells, those able to capture antigen via surface Ig and best present it on surface MHCII, are selected by follicular helper T (Tfh) cells (Victora and Nussenzweig, 2012). The strength of interaction between Tfh cells and GC B cells, which is proportional to the

amount of antigen presented by GC B cells, drives the cyclic reentry and determines the cell cycle speed and number of divisions of GC B cell clones (Victora et al., 2010; Gitlin et al., 2014; Shulman et al., 2014).

Follicular regulatory CD4+ T (Tfr) cells, a population of regulatory T (Treg) cells, express the transcription factor *Bcl6* and chemokine receptor *CXCR5* and localize to the follicle and the GC following infection or immunization (Linterman et al., 2011; Chung et al., 2011; Wollenberg et al., 2011). Tfr cells suppress excessive immune responses, such as those occurring in autoreactivity, through a process mediated by the inhibitory co-receptor CTLA-4 (Wing et al., 2014; Sage et al., 2014). However, the role of Tfr cells in regulating antigen-specific B cell selection within the GC is currently unclear. The existing paradigm suggests that Tfr cells are inhibitory and restrain overall GC responses, including antigen-specific B cell responses (Wing et al., 2014; Clement et al., 2019; Sage et al., 2016). In contrast, other groups have reported no obvious effect on antigen-specific antibody responses in the absence of Tfr cells (Fu et al., 2018; Botta et al., 2017). Elucidating the regulatory function of Tfr cells in

[1]Department of Immunobiology, Yale University School of Medicine, New Haven, CT; [2]Interdepartmental Program in Computational Biology and Bioinformatics, Yale University School of Medicine, New Haven, CT; [3]Department of Microbiology, Icahn School of Medicine at Mount Sinai, New York, NY; [4]Department of Microbiology, Perelman School of Medicine, University of Pennsylvania, Philadelphia, PA; [5]Department of Biostatistics, Yale School of Public Health, New Haven, CT; [6]Department of Microbiology and Immunology, University of Gothenburg, Gothenburg, Sweden; [7]Department of Neurology, Yale University School of Medicine, New Haven, CT; [8]Department of Pathology, Yale University School of Medicine, New Haven, CT; [9]Department of Internal Medicine (Rheumatology, Allergy, and Immunology), Yale University School of Medicine, New Haven, CT.

Correspondence to Joe Craft: joseph.craft@yale.edu.

modulating antigen-specific B cell responses using physiologically relevant models has fundamental implications for our understanding of the selection process occurring within the GC.

Treg cells can suppress immune-mediated inflammation and self-reactive autoimmune diseases (Josefowicz et al., 2012). They also promote optimal immune responses by actively maintaining homeostasis. For example, Treg cells are necessary for the homeostatic priming of the CD8$^+$ T cell response by increasing the avidity of the primary response (Pace et al., 2012). Treg cells also promote CD8$^+$ T cell memory maturation by actively dampening inflammation during the resolution course of infection, aiding a return to homeostasis (Laidlaw et al., 2015, 2016; Kalia et al., 2015). In line with these findings, we previously demonstrated that Tfr cell–derived IL-10 was necessary to maintain the GC B cell response following acute infection of lymphocytic choriomeningitis virus (Laidlaw et al., 2017).

Based on these observations, we hypothesized that Tfr cells might promote the selection of antigen-specific B cell responses, and accordingly, promote GC B cell output. We find that Tfr cells promote antigen-specific GC B cell responses during influenza viral challenge, with development of plasma cells and effective humoral memory. These findings indicate that Tfr cells optimize GC responses and regulate B cell recall responses, thus enhancing our understanding of the role of Tfr cells in vaccine-induced immunity, important in the optimization of vaccine development strategies.

Results

### Tfr cells promote the antigen-specific B cell response during the late course of influenza virus infection

To test the role of Tfr cells in regulating antigen-specific GC responses, we infected C57BL/6 mice with a mouse-adapted strain of influenza virus, A/Puerto Rico/8/1934 H1N1 (PR8), and isolated lymphocytes from the relevant draining mediastinal LNs (mLNs) at various time points following infection. Consistent with published studies (Botta et al., 2017), Tfr cell numbers peaked at day 30 following infection, at which time total GC B cells and antigen-specific GC B cells also reached maximum numbers (Fig. S1, A, C, and D); Tfh cell numbers peaked earlier, at day 12 post infection (p.i.; Fig. S1 B). We generated mice that specifically lack Tfr cells (Bcl6$^{f/f}$ Foxp3-Cre) and confirmed their depletion at both early and late time points following infection, day 8 and day 40 p.i., respectively (Fig. S1 E). Bcl6$^{f/f}$ Foxp3-Cre animals displayed no sign of overt disease at steady state and did not show differences in the basal number of GC B cells, Tfh cells, or Treg cells in the spleen compared with their littermate controls (Fig. S1 F).

To investigate whether the GC response was affected in the absence of Tfr cells, we isolated lymphocytes from mLNs of Tfr cell–deficient (Bcl6$^{f/f}$ Foxp3-Cre) and control (Bcl6$^{f/f}$) animals at day 38 p.i. This time point was chosen with the rationale that the GC response might be affected the most in the absence of Tfr cells following their numerical peak at day 30 p.i. The percentage and number of B cells with a GC phenotype (GL7$^+$CD38$^-$ of B220$^+$IgD^{low} population) were comparable between the two

groups of mice (Fig. 1 A). The GC sizes were also similar as determined by confocal imaging of the mLN sections (Fig. 1 B). We then assessed the GC B cells that have specificity for the influenza virus surface glycoprotein hemagglutinin (HA). There was a marked decrease in percentage as well as number of HA-specific GC B cells as measured by recombinant HA probes, which have a mutation in the sialic acid binding site (Tyr98Phe) to prevent nonspecific binding to sialic acid on the cell surface (Fig. 1 C; Angeletti et al., 2017; Whittle et al., 2014). The transcriptomes of HA-specific GC B cells were similar between the Tfr cell–deficient and –sufficient groups (Fig. 1 D). The viral loads in Tfr cell–deficient (Bcl6$^{f/f}$ Foxp3-Cre) and control (Bcl6$^{f/f}$) animals were also comparable at both day 5 and day 9 p.i., suggesting that the numerical difference in antigen-specific GC B cells between the two groups was not due to differences in viral load or viral clearance (Fig. 1 E).

As GC B cells give rise to high-affinity, antibody-producing plasma cells, we next sought to determine whether the antigen-specific plasma cell compartment was impaired in the absence of Tfr cells following influenza virus infection. We quantified HA-specific antibody-secreting cells (ASCs) using ELISPOT assays. ELISPOT analysis of bone marrow cells showed that there was a statistically significant reduction in the number of HA-specific ASCs in the Tfr cell–deficient animals compared with that in the controls, despite comparable numbers of total bone marrow cells between the two groups (Fig. 2 A). The intensity of the spots was also reduced in the absence of Tfr cells, as shown by the representative images of ELISPOT assays. This suggests the possibility that the antigen-specific antibodies produced per ASC are reduced in the absence of Tfr cells or that their affinity is lower in Tfr cell–deficient animals.

While serum antibodies produced early in an immune response are mainly derived from short-lived plasmablasts generated as part of an extrafollicular response, those from later time points are mostly produced by ASCs developed via GCs (Nutt et al., 2015). We next evaluated antigen-specific antibody responses by assessing titers of antibodies to the influenza virus HA using quantitative ELISA. We found that while the induction of HA-specific IgG antibodies was similar between Bcl6$^{f/f}$ Foxp3-Cre and Bcl6$^{f/f}$ controls at day 15 p.i., IgG antibodies targeting HA were significantly reduced in mice lacking Tfr cells relative to controls at day 36 p.i. (Fig. 2 B). Consistently, Tfr cell–deficient mice had significantly lower titers of HA-specific Ig isotypes IgG1 and IgG2a (IgG2c in C57BL/6 animals) than those in their wild-type counterparts (Fig. 2 C). We next asked whether this phenomenon was unique to the antigen HA. We measured antibody responses to neuraminidase (NA), the second most abundant surface glycoprotein of influenza virus, which also contributes to protection from influenza virus infection (Chen et al., 2018). Likewise, NA-specific IgG antibody titers were reduced in Tfr cell–deficient mice relative to the controls at day 36 p.i. (Fig. 2 D). Thus, mice that lacked Tfr cells had decreased antigen-specific antibody titers, which was consistent with the reduction in antigen-specific GC B cells and plasma cells. Tfr cell–deficient mice also had reduced affinity of anti-HA IgGs compared with wild-type controls (Fig. 2 E). We observed the same comparative reductions in antigen-specific GC B cells and
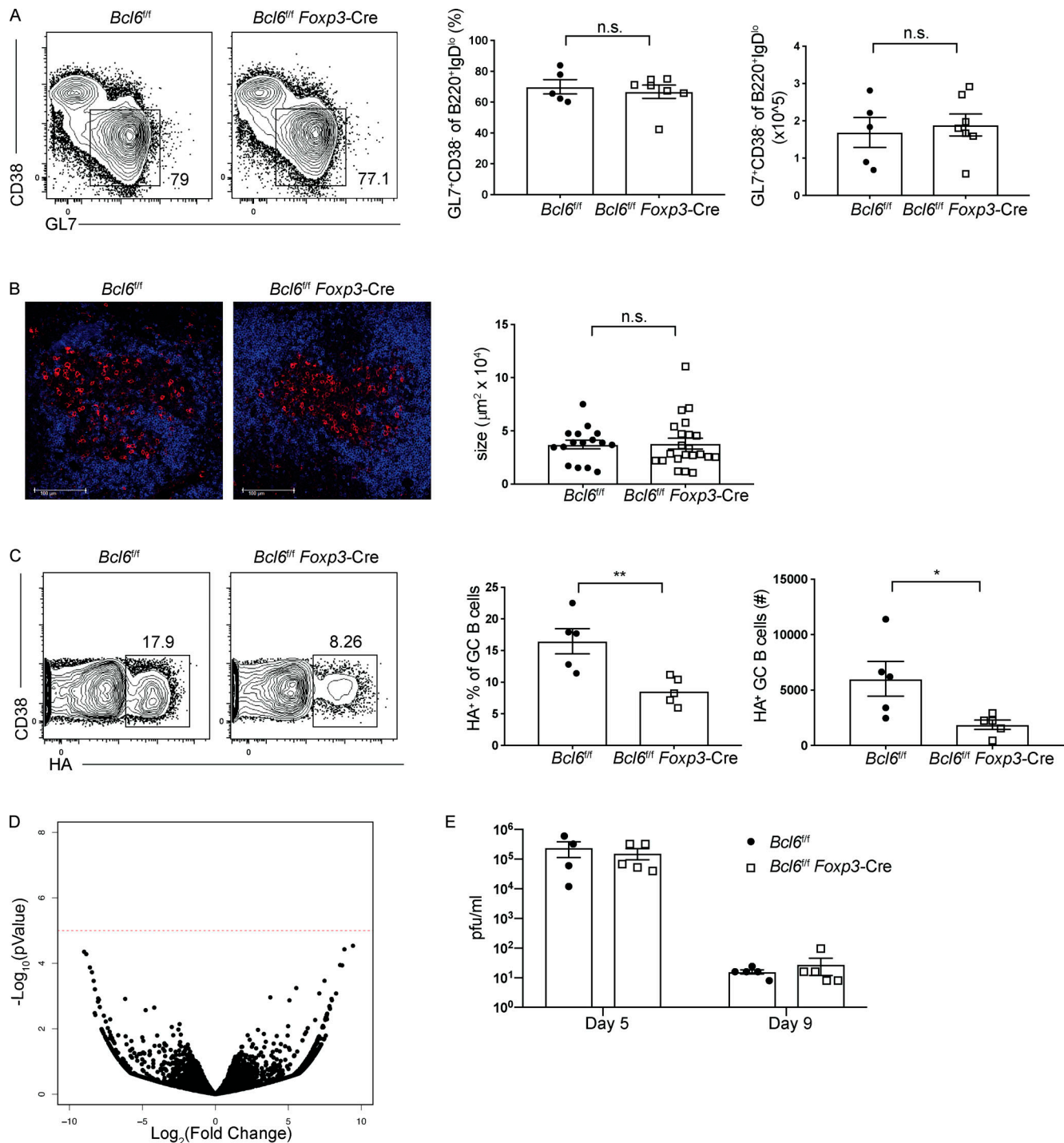
Figure 1. **Mice lacking follicular regulatory CD4+ T cells have reduced antigen-specific GC responses.** Analysis of the GC B cell responses in *Bcl6*[f/f] and *Bcl6*[f/f] *Foxp3*-Cre mice at the late time point following influenza virus infection. **(A)** Left: Representative plots of the GC B cell responses in *Bcl6*[f/f] or *Bcl6*[f/f] *Foxp3*-Cre mice at day 38 p.i. Right: Frequency and number of cells as indicated by the gates shown on the left. **(B)** Representative confocal images of the GCs from *Bcl6*[f/f] or *Bcl6*[f/f] *Foxp3*-Cre mice at day 36 p.i. IgD shown in blue and peanut agglutinin shown in red. Right: GC sizes as measured by ImageJ. Scale bar, 100 μm. **(C)** Left: Representative plots of HA-specific GC B cells at day 38 p.i. The cells were gated on GL7+ CD38− GC B cells of the B220+IgM−IgD[low] population. Right: Frequency and absolute numbers of HA-specific GC B cells. **(D)** RNA-seq analysis of HA+ GC B cells from *Bcl6*[f/f] and *Bcl6*[f/f] *Foxp3*-Cre mice at 36 d following influenza virus infection. Volcano plot of -$\log_{10}$ P value vs. $\log_2$ fold change of the most differentially expressed 5,000 genes. The dashed line plotted indicates the level of Bonferroni-corrected P value <0.05. No gene is found to show significance change with adjusted P value <0.05. **(E)** Plaque assay measuring viral load in *Bcl6*[f/f] and *Bcl6*[f/f] *Foxp3*-Cre mice at day 5 and day 9 p.i. Statistical analyses were performed using the unpaired two-tailed Student's *t* test (*, P < 0.05; **, P < 0.01). Data for A and C are from one experiment representative of four experiments with five to seven mice per group. Data for B and E are from one experiment representative of two experiments with three to five mice per group. Data for D are from two independent experiments with three to four mice per group pooled for each sample. n.s., not significant.
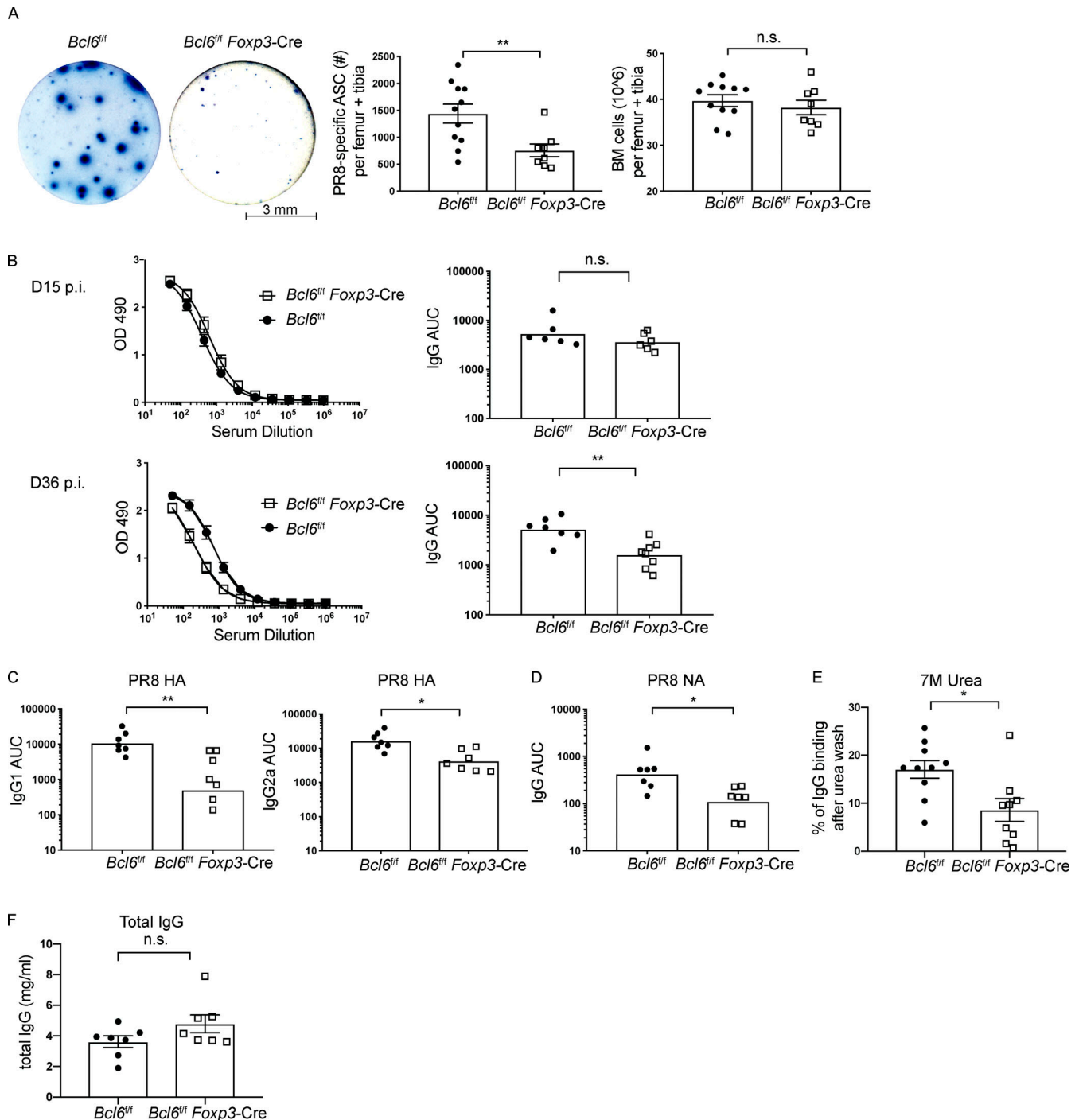
Figure 2. **CD4+ Tfr cells are important for antigen-specific plasma cell and antibody responses following influenza virus infection. (A)** Left: Representative image from ELISPOT of HA-specific IgG ASCs. Right: Quantification of HA+ ASCs and total bone marrow cells of *Bcl6*f/f or *Bcl6*f/f *Foxp3*-Cre mice at day 38 p.i. Scale bar, 3 mm. **(B)** ELISA analysis of serum influenza-specific antibody titers in Tfr cell–deficient (*Bcl6*f/f *Foxp3*-Cre) and wild-type (*Bcl6*f/f) mice at various time points following infection with PR8. At day 15 p.i. (top) and day 36 p.i. (bottom), HA-specific IgG in sera from two groups of mice were quantified by ELISA. **(C)** Representative plots of quantification of HA-specific IgG1 (left) and HA-specific IgG2a (right) from *Bcl6*f/f *Foxp3*-Cre and control mice. **(D)** Representative plot of NA-specific IgG. **(E)** Affinity measurements of *Bcl6*f/f or *Bcl6*f/f *Foxp3*-Cre mice at day 36 p.i. determined by 7 M urea ELISA, expressed as percentage of IgG bound to HA treated by 7 M urea divided by untreated IgG bound. **(F)** The concentration of total IgG in the sera from Tfr cell–deficient (*Bcl6*f/f *Foxp3*-Cre) and wild-type (*Bcl6*f/f) mice at day 36 p.i. Statistical analyses were performed using the unpaired two-tailed Student's *t* test (*, P < 0.05; **, P < 0.01). Data for A are pooled from two experiments representative of four or five experiments with four to six mice per group performed day 38 p.i. with PR8. Data for B–D and F are from one experiment representative of three experiments with five to eight mice per group. Data for E are pooled from two independent experiments with four to six mice per group. AUC, area under the curve; BM, bone marrow; n.s., not significant.

antibody responses in *Bcl6*^{f/f} *Foxp3*-Cre animals when we used *Foxp3*-Cre littermates as controls (Fig. S2, A and B).

The total serum IgG concentrations were higher in the Tfr cell–deficient animals compared with the controls, though the differences did not reach statistical significance (Fig. 2 F). We did not detect serum anti-nuclear antibody (ANA) responses in the absence of Tfr cells following influenza virus infection or in steady state with a serum dilution of 1:20 (Fig. S3, A and B). However, with a serum dilution of 1:5, we observed weak positive staining using sera from Tfr cell–deficient animals, but not those from control animals following infection or in steady state from either group (Fig. S3, C and D). Blinded scoring of ANA staining revealed that the Tfr cell–deficient group had higher positivity scores compared with those of the control group (Fig. S3 E; Peng and Craft, 2020).

Adoptive transfer of Treg cells rescues impairment in the antigen-specific GC B cell response

These data demonstrated that Tfr cells promote antigen-specific B cell responses during GC development. To further validate that Tfr cells are sufficient for the optimal influenza virus–specific GC B cell response, we adoptively transferred sorted CD4+Foxp3+ Treg cells from congenically marked naive Treg cell reporter animals (Foxp3^{EGFP} CD45.1+) into the *Bcl6*^{f/f} *Foxp3*-Cre group 1 d before influenza virus infection with the idea that Treg cells differentiate into Tfr cells upon infection (Fig. 3 A). We could not adoptively transfer Tfr cells as we were limited by their number obtained during influenza virus infections. We observed that the adoptive Treg cell transfer restored HA-specific GC B cells in *Bcl6*^{f/f} *Foxp3*-Cre mice, both in percentage and number, to levels comparable to those in *Bcl6*^{f/f} control mice at day 40 p.i. (Fig. 3 B). Additionally, we did not observe the transferred Treg cells transdifferentiate into Tfh cells (Fig. 3 C). We confirmed that the transferred Treg cells differentiated into Tfr cells in the *Bcl6*^{f/f} *Foxp3*-Cre animals (Fig. 3 D). These results demonstrate that Treg cells and most likely Tfr cells are important for the optimal antigen-specific GC B cell responses.

Polyclonal and antigen-specific Tfh cell responses are not affected in the absence of Tfr cells

In addition to affecting GC B cells, Tfr cells have the potential to influence the Tfh cell population. We assessed the Tfh cell response in mLNs at day 8 and day 38 following influenza virus infection. Tfh cells were gated as CD4+CD44^{hi}Foxp3−Ly6C^{lo}Psgl-1^{lo} PD-1^{hi}CXCR5^{hi} (Marshall et al., 2011; Crotty, 2011). At day 8 p.i., although the percentage of Tfh cells in mice that lacked Tfr cells was reduced compared with control mice, their absolute numbers were comparable between the two groups (Fig. S4 A). The expressions of the lineage-defining transcription factor *Bcl6* and proliferation marker *Ki67* were similar between the two groups (Fig. S4 B). RNA sequencing (RNA-seq) analysis revealed top differentially expressed genes not typically expressed by T cells, and thus we concluded there was no apparent difference in gene expression profiles of Tfh cells in *Bcl6*^{f/f} *Foxp3*-Cre and *Bcl6*^{f/f} control mice at this time point (Fig. S4 C and Table S1). HA-specific and nucleoprotein (NP)-specific Tfh cell percentages and numbers were also similar between the Tfr cell–sufficient and Tfr cell–deficient

groups (Fig. S4 D). During the late course of infection, at day 38 p.i., both the percentages and absolute numbers of Tfh cells were similar between the Tfr cell–sufficient and Tfr cell–deficient groups (Fig. S4 E). These data indicate that the Tfh cell response is not affected by the lack of Tfr cells during influenza virus infection. Additionally, both the percentages and absolute numbers of Treg cells were similar between the Tfr cell–sufficient and Tfr cell–deficient groups at day 9 and day 38 p.i. (Fig. S4, F and G), suggesting that total Treg cells are not affected by the lack of Tfr cells following infection.

Tfr cell–deficient mice use distinct V_H (variable region of the heavy chain) genes compared with their wild-type counterparts following influenza virus infection

To explore whether the B cell receptor (BCR) repertoire was altered in the absence of Tfr cells, we performed high-throughput BCR repertoire profiling. We sorted GC B cells from mLNs of *Bcl6*^{f/f} *Foxp3*-Cre and *Bcl6*^{f/f} control animals at day 15 p.i., as well as naive follicular B cells from mLNs of uninfected animals, and performed high-throughput sequencing of the BCR heavy chain mRNA. This approach minimizes PCR bias and consequence of errors introduced by sequencing as previously described (Vander Heiden et al., 2014). We analyzed ~5,468, 5,399, and 561 reconstructed unique and error-corrected *Igh* sequences that passed quality control from *Bcl6*^{f/f} *Foxp3*-Cre, *Bcl6*^{f/f}, and naive, uninfected animals, respectively (Table S2). Principal component analysis revealed that the V_H gene usage in BCR sequences of follicular B cells from naive animals clustered separately from those of GC B cells from infected animals (Fig. 4 A). Moreover, Tfr cell–deficient and Tfr cell–sufficient mice showed distinct V_H gene usage signatures following infection (Fig. 4, A and B; and Fig. S5 A). Several V_H genes were differentially expressed in the *Bcl6*^{f/f} *Foxp3*-Cre animals compared with *Bcl6*^{f/f} controls. Compared with their wild-type counterparts, the frequencies of genes *IGHV1-66* and *IGHV5-17* were significantly lower in Tfr cell–deficient animals (Fig. 4 C).

We next investigated the significance of differential V_H gene usage in the absence of Tfr cells by reanalyzing Sanger-based sequencing of B cells from recombinant HA-immunized mice in a published study (Kuraoka et al., 2016). Notably, the V_H genes that were differentially expressed between *Bcl6*^{f/f} *Foxp3*-Cre and *Bcl6*^{f/f} control mice following infection were positively correlated with the V_H genes enriched following HA immunization as assessed by Pearson correlation analysis (Fig. 4 D). No statistically significant correlation with the expanded V_H genes in response to anthrax protective antigen (PA), an irrelevant antigen control, was detected (Fig. 4 D). Other features of the repertoire analysis appeared to be similar between the two groups following influenza virus infection, including clonality, selection pressure, isotype usage, and somatic hypermutation (Fig. S5, B–F). We therefore reasoned that Tfr cells were able to shape the B cell repertoire following infection by selecting for B cells that use specific BCR sequences known to be involved in antigen-specific responses.

Sequential vaccination with partially conserved antigens reveals that Tfr cells promote effective memory formation

Immunological memory is crucial for B cell responses to influenza virus in humans (Andrews et al., 2015). Since the specificity of
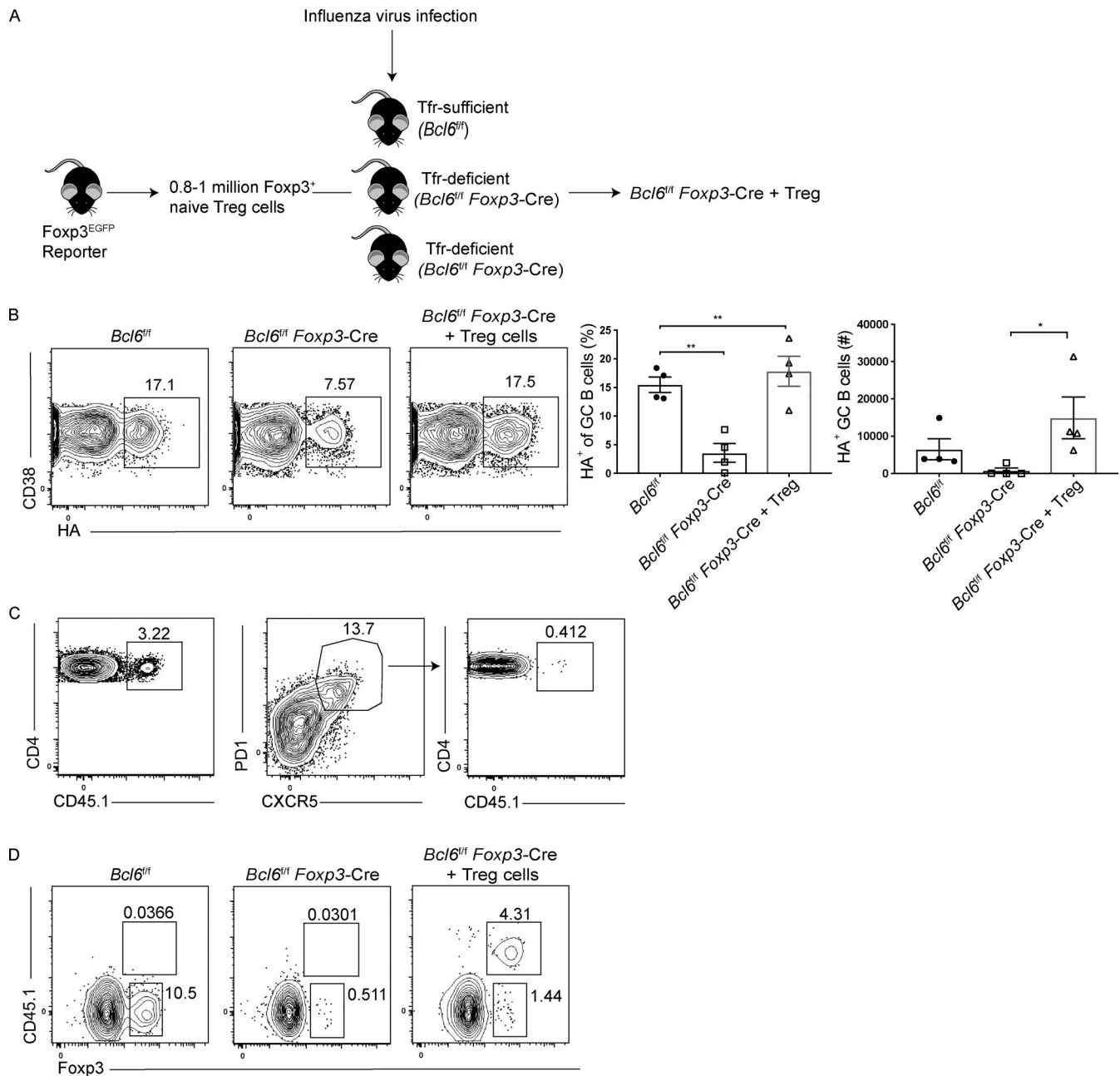
Figure 3. **Adoptive transfer of regulatory CD4+ T cells rescues impairment in antigen-specific B cell responses. (A)** Schematic for the Treg cell adoptive transfer experiment. **(B)** Left: Representative plots of HA-specific GC B cells as determined by HA probe in *Bcl6*[f/f], Bcl6[f/f] *Foxp3*-Cre, and Bcl6[f/f] *Foxp3*-Cre + Treg cell group. Right: Quantification of the percentages and numbers of HA-specific GC B cell responses with adoptive transfer strategy at day 38 p.i. **(C)** Left: Representative plot of the adoptively transferred Treg cell population defined as CD4+CD44^{hi}CD45.1+. Middle and right: Representative plots of the adoptively transferred population (CD45.1+) in the Tfh cell compartment defined as CD4+CD44^{hi}Foxp3−Ly6C−PSGL1^{low}CXCR5^{hi}PD1^{hi}. **(D)** Representative plots of Tfr cells derived from the transferred Treg cells gated as CD45.1+ Foxp3+ in *Bcl6*[f/f], Bcl6[f/f] *Foxp3*-Cre and Bcl6[f/f] *Foxp3*-Cre + Treg cell animals. Tfr cells are defined as CD4+CD44^{hi}Ly6C−PSGL1^{lo}CXCR5^{hi}PD1^{hi}Foxp3+. Statistical analyses were performed using the unpaired two-tailed Student's *t* test (*, P < 0.05; **, P < 0.01). Data are from one experiment representative of two experiments with four or five mice per group performed 38 d following influenza virus infection.

the primary response affects secondary responses, impaired antigen-specific B cell primary responses in the absence of Tfr cells could lead to defective memory responses. To investigate this possibility, we used a sequential vaccination model with repeated exposure of antigenically distinct strains of influenza viruses which shared the conserved immunosubdominant

stalk domain of the glycoprotein HA to induce stalk-specific antibody responses (Nachbagauer et al., 2017; Nachbagauer and Palese, 2020; Choi et al, 2019). We immunized Tfr cell–deficient and –sufficient mice with H1N1 intramuscularly, followed by a boost with a laboratory reassortant strain, H5N1, at day 42 after priming and then a second boost with another
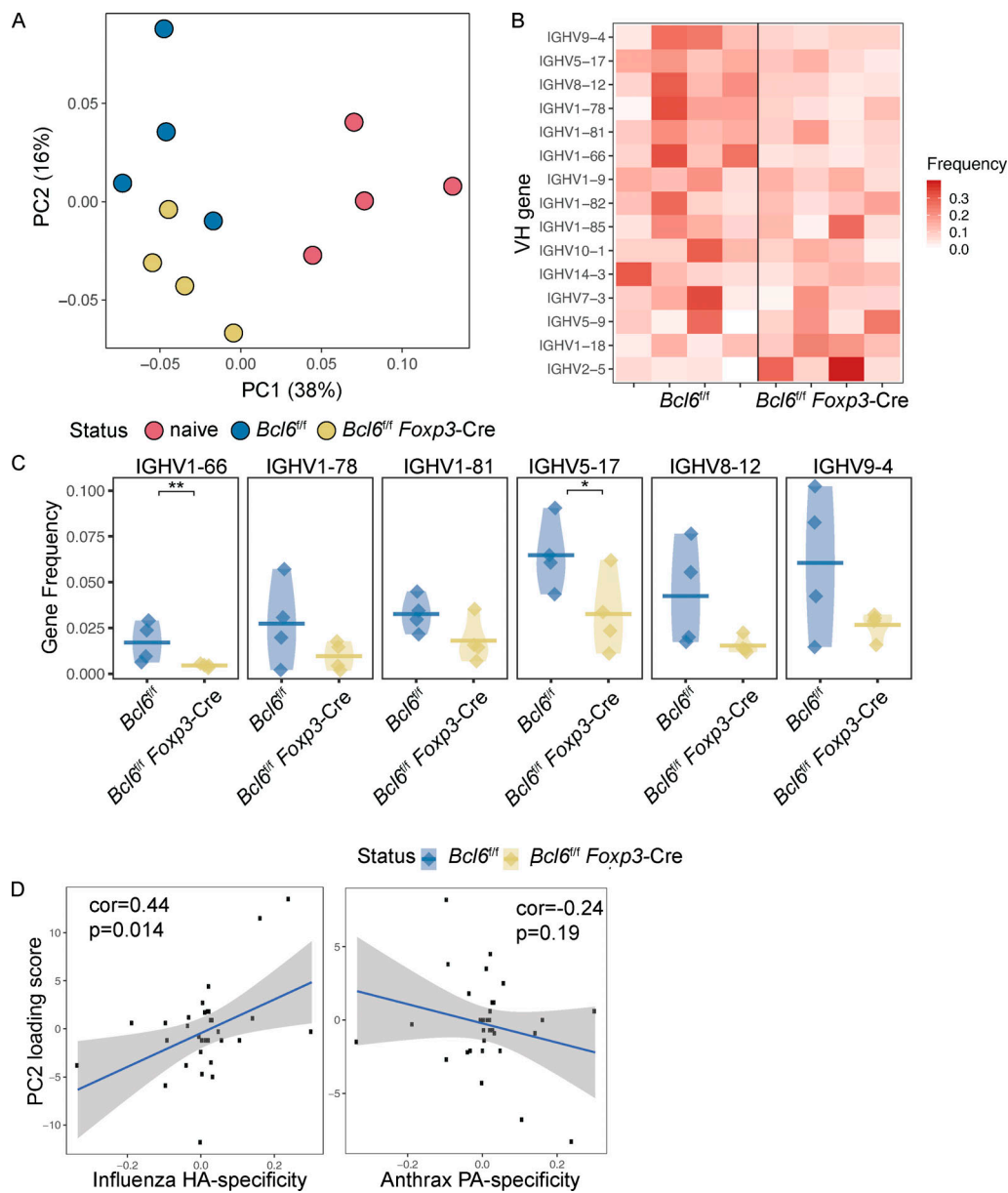
Figure 4. **Mice lacking follicular regulatory CD4+ T cells exhibit a distinct BCR repertoire following influenza virus infection. (A)** Principal component analysis visualization of V_H gene usage frequency for total unique *Igh* sequences isolated from the mLN-derived repertoire. **(B)** Heatmaps showing V_H gene usage frequencies for the top 15 V_H genes based on maximal principal component 2 score from principal component analysis of total Igh sequences. These are shown with values normalized for each row based on Z-score. **(C)** Individual V_H gene frequencies relative to the total number of unique variant VDJ sequences are plotted for the top six V_H genes. Significance was assessed using a two-tailed Wilcoxon test with a significance threshold of *, $P < 0.1$; **, $P, < 0.05$. Horizontal bars show the average frequency of V_H gene usage for samples of a specific genotype. **(D)** Scatterplots for V_H genes based on their principal component 2 loading score compared with their usage frequency among the published set of V_H sequences from Kuraoka et al. (2016) associated with HA specificity (compared with non-HA specifics; left) or with PA specificity (compared with non-PA specific sequences; right) at day 16 after immunization. Correlations were computed as Pearson correlation coefficients, and a P value was assigned to the significance of the correlation with a significance threshold of $P < 0.05$. For the BCR repertoire analysis, data are from one experiment with four mice per group performed 15 d following PR8 influenza virus infection. Cor., Pearson correlation coefficient.

reassortant strain, H6N3, at day 84 (Fig. 5 A). These three viral strains (all influenza A group 1 viruses) have divergent HA head domains but share a similar conserved stalk domain. Thus, following each boost with a heterologous strain, the animals mount primary responses toward the head domains (to which they are naive), while reexposure to the conserved stalk domain can boost memory response toward this domain (Nachbagauer and Palese, 2020).

We measured memory responses by detecting stalk-reactive antibodies in *Bcl6^f/f Foxp3*-Cre and *Bcl6^f/f* control animals. As previously described, we performed stalk-specific ELISAs using a chimeric HA cH11/1 comprising an H11 head domain (to which mice were not exposed) and an H1 stalk domain as substrate (Nachbagauer et al., 2014). The reactivity measured by ELISA toward this substrate is predominantly specific to the H1 stalk
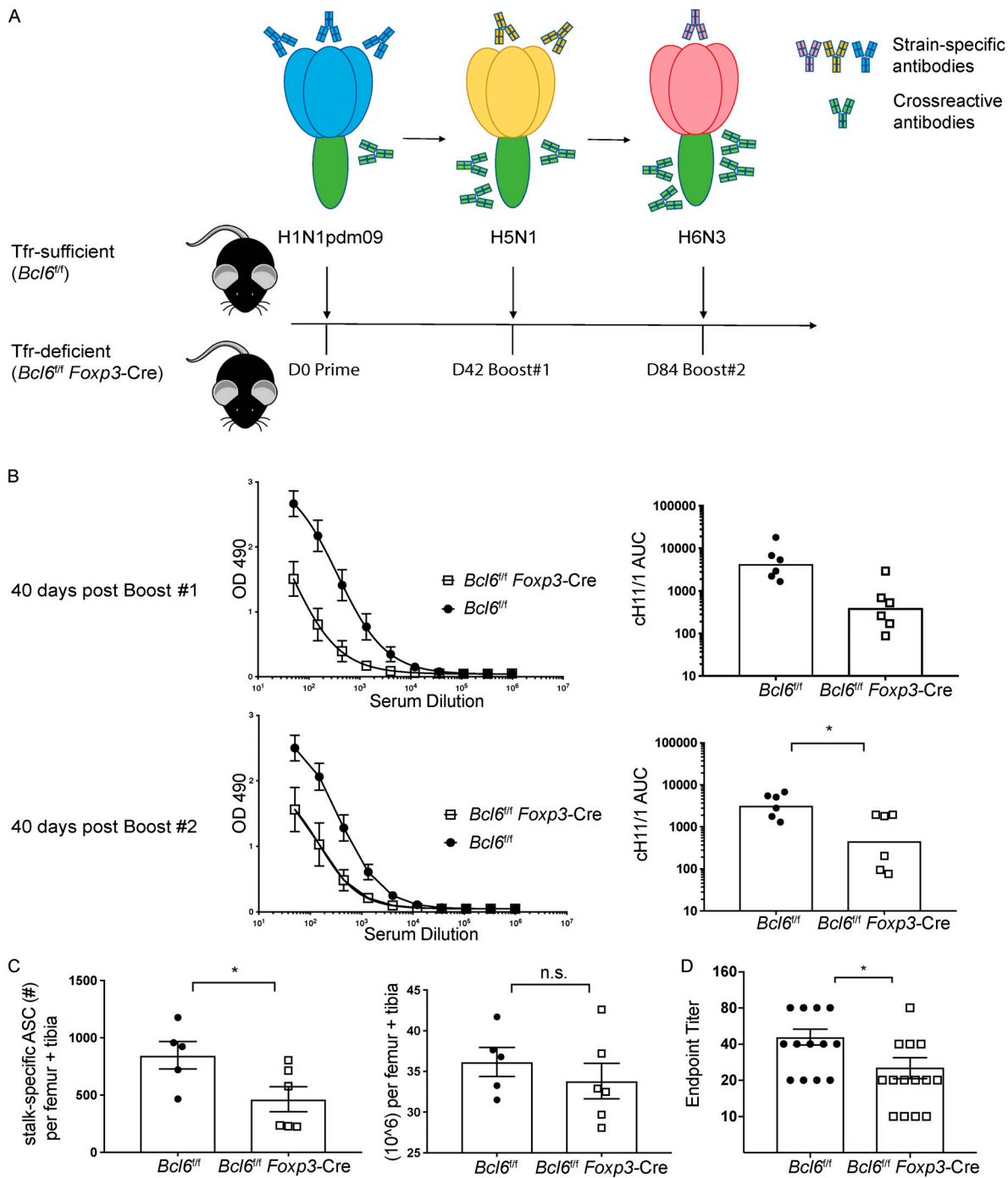
Figure 5. **Mice generate impaired influenza virus stalk-specific B cell responses in the absence of follicular regulatory CD4⁺ T cells in a sequential vaccination model with antigenically diverse antigens.** Analysis of the stalk-specific B cell response in $Bcl6^{f/f}$ $Foxp3$-Cre and $Bcl6^{f/f}$ mice following multiple boosts in an influenza virus sequential vaccination model. **(A)** Schematic of the sequential vaccination model. **(B)** Quantification of stalk-specific IgG antibody titers as determined by ELISA using chimeric HA cH11/1 as coating substrate at 40 d following the first boost (top) and 40 d following the second boost (bottom). **(C)** Left: Quantification of stalk-specific ASCs in the bone marrow compartment from $Bcl6^{f/f}$ or $Bcl6^{f/f}$ $Foxp3$-Cre mice at 42 d following the second boost. Right: Quantification of the total number of bone marrow cells in each mouse. **(D)** Antibody response against the H1N1 head domain in $Bcl6^{f/f}$ $Foxp3$-Cre and $Bcl6^{f/f}$ mice measured by influenza hemagglutination inhibition assay following sequential vaccination. Statistical analyses were performed using the unpaired two-tailed Student's t test (*, P < 0.05). Data for A–C are from one experiment representative of two experiments with five to seven mice per group performed at various time points following sequential vaccination with diverse group 1 influenza viruses. Data for D are pooled from two independent experiments with five to seven mice per group following sequential vaccination. AUC, area under the curve; n.s., not significant.

Lu et al.
Tfr cells promote humoral memory

Journal of Experimental Medicine   8 of 14
https://doi.org/10.1084/jem.20200547

domain. At day 40 after the first boost, Tfr cell–deficient mice showed a trend of reduced HA stalk–specific IgG titers compared with their wild-type counterparts (Fig. 5 B). This difference between the two groups of animals became statistically significant following the second boost (Fig. 5 B). The increase of anti-stalk antibody response following the second boost was not dramatic and could represent a "ceiling effect" that has been observed previously in chimeric HA-based vaccine studies, which used sequential immunization with vaccine strains expressing the conserved HA stalk domain and exotic HA heads (Nachbagauer et al., 2016). Consistent with reduced HA stalk–specific serum IgG titers, Tfr cell–deficient mice also had significantly impaired HA stalk–specific plasma cells compared with their wild-type counterparts as determined by HA stalk–specific ELISPOT assay, while the numbers of total bone marrow cells were similar between the two groups (Fig. 5 C). Sera from both Tfr cell–deficient and –sufficient animals showed comparable weak ANA staining at 40 d after the second boost (data not shown), possibly due to advanced age of the animals at the end of the experiments. HA head–specific antibody titers, measured by hemagglutination inhibition assay, which assesses the antibodies against the HA head domain (Jacobsen et al., 2017), were also reduced in Tfr cell–deficient animals compared with their wild-type littermates (Fig. 5 D). This is consistent with the observation that animals had impaired primary responses in the absence of Tfr cells. These data indicate that Tfr cells promote productive antigen-specific humoral memory responses in response to heterologous influenza infections.

Discussion

We found that Tfr cells support influenza virus–specific B cell responses to infection and vaccination. In the absence of Tfr cells, influenza virus–specific GC B cells, LLPCs, and antibody titers are significantly reduced. We discovered an altered BCR repertoire following infection in mice lacking Tfr cells, which may account for a reduction in the expanded influenza virus–specific B cells. The impaired primary response then further leads to impaired humoral memory responses following heterologous influenza virus vaccinations.

Previous studies have explored the role of Tfr cells in modulating antigen-specific responses in the setting of influenza virus infection, with results showing that anti–influenza virus antibodies and plasma cells did not appear to be different between Tfr cell–deficient and Tfr cell–sufficient animals (Botta et al., 2017; Fu et al., 2018). These two studies assessed antigen-specific B cell responses at day 9 and day 30 following infection, respectively. At day 9 p.i., the difference between the two groups was still not detectable in our experiments. At day 30 p.i., there was a trend of reduced influenza virus–specific plasma cells in *Bcl6*f/f *Foxp3*-Cre animals compared with controls in the published work (Botta et al., 2017), which is consistent with our data supporting a role for Tfr cells at late time points following infection (36 d p.i. and beyond). The kinetics also correspond well with the number of Tfr cells peaking at 30 d following influenza virus infection.

Our finding contrasts with previous studies, in which Tfr cells were found to suppress antigen-specific B cell responses (Sage et al., 2016; Clement et al., 2019). In the latter examples, both the in vitro and in vivo experiments were done following immunization with the antigen NP-OVA (protein-hapten conjugate), with the insight gained from these studies serving as an important foundation upon which we build. It is likely that the function of Tfr cells depends on the complexity of the antigen, and the timing. We reason that in live viral infection, such as with influenza virus, a complex antigen with distinct epitopes and antigen persistence due to replication, the maintenance of diverse B cell clones, both antigen-specific and non–antigen-specific, is distinct from those in an immunization model with simpler antigens (Tas et al., 2016).

The Cre/LoxP system can have infidelity issues, as has been observed (Schmidt-Supprian and Rajewsky, 2007). To confirm that the phenotype was not due to leakiness of Cre recombinase, we conducted adoptive transfer experiments in which Treg cells rescued the impairment of antigen-specific GC B cells in the Tfr cell–deficient animals, suggesting that the lack of Tfr cells is responsible for the phenotype. Furthermore, the analyses of Tfh cells at day 8 p.i. and day 38 p.i. did not reveal differences in numbers of Tfh cells, confirming that they were not affected in this Cre system. Overall, we exclude the possibility of Cre leakiness causing impaired antigen-specific GC B cell responses.

An impaired antigen-specific humoral response was also not due to differences in viral load or viral clearance, as viral titers were similar between the Tfr cell–deficient and –sufficient groups at various time points. Additionally, in the sequential vaccination experiments, the route of immunization was intramuscular. The virus is not able to complete more than one replication cycle due to the lack of specific host proteases in the muscle tissue, which are required for cleavage of the influenza virus surface HA (Böttcher-Friebertshäuser et al., 2010). Therefore, we argue that virus clearance does not play a role in the measured antibody response in this setting as well.

It seems intuitive and evolutionarily sensible to have regulatory cells participating in GC responses to optimize the output, which is antigen-specific high-affinity responses. Yet how do Tfr cells achieve that goal? One possibility is that Tfr cells preferentially suppress non–antigen-specific GC B cells while sparing the antigen-specific ones. This would be reminiscent of the role played by Treg cells in optimizing CD8+ T cell responses: Treg cells preferentially suppress responses by T cells that have weak, lower-affinity interactions with their cognate antigen (also the reason that Treg cells control self-reactive T cells due to their low-affinity) while sparing high-affinity interactions (Pace et al., 2012). One can imagine a similar scenario for the GC selection process of antigen-specific B cells regulated by Tfr cells. Specifically, as the positive selection signal is directly proportional to the strength of interaction between Tfh cells and GC B cells, Tfr cells can selectively inhibit non–antigen-specific GC B cells based on their low-strength interactions with Tfh cells, whereas antigen-specific GC B cells that engage in high-strength interactions with Tfh cells can overcome this suppression. The expression of positive selection signals, such as mTORC and cMyc signaling, which are up-regulated in GC B cells having

recently received Tfh cell help, is likely to serve as a proxy for the strength of interaction that can be regulated by Tfr cells (Dominguez-Sola et al., 2012; Ersching et al., 2017). Furthermore, overproliferation and outgrowth of non–antigen specific B cell clones in the absence of Tfr cells can compete for limited Tfh cell help within a given GC, therefore resulting in impaired antigen-specific B cell responses.

It will be of interest to identify Tfr cell–derived molecules (e.g., cytokines, surface molecules) that might mediate the aforementioned process of optimizing antigen-specific B cell responses within the GC. We explored one Tfr cell–derived molecule, IL-10, which does not affect the level of influenza virus–specific B cell response or polyclonal Tfh cell response (data not shown). It will be important for future work to focus on specific Tfr cell–derived molecules and elucidate their functions in modulating different aspects of productive GC responses. In summary, our study reveals a novel function of Tfr cells in promoting antigen-specific B cell responses following influenza virus infection. Targeting Tfr cells or Tfr cell–derived molecules may provide more effective vaccine development strategies in the future.

Materials and methods

Design
The objective of this study was to determine the role of Tfr cells in regulating antigen-specific B cell responses following influenza virus infection. Tfr cell–deficient and Tfr cell–sufficient mice were subjected to influenza virus infections or immunizations. The antigen-specific B cell responses were assessed by flow cytometry, ELISPOT, ELISA, and BCR sequencing. Detailed methods are described in the sections below. Control and experimental groups were sex and age matched. Littermates were used for all experiments where possible. The investigators were not blinded. The sample sizes and experimental replications are indicated in the figure legends.

Mice
C57BL/6 mice were purchased from the National Cancer Institute or The Jackson Laboratory. C.Cg-Foxp3^{tm2Tch}/J ($Foxp3^{EGFP}$), B6.129(FVB)-Bcl6$^{tm1.1Dent}$/J ($Bcl6^{f/f}$), B6.129 (Cg)-Foxp3$^{tm4(YFP/cre)}$Ayr/J ($Foxp3$-Cre), and B6.129P2(C)-Cd19$^{tm1(cre)Cgn}$/J mice were purchased from The Jackson Laboratory. $Il10^{f/f}$ mice (Roers et al., 2004) have been described. $Il10ra^{f/f}$ mice were generated by the Flavell laboratory as previously described (Laidlaw et al., 2015). All animal experiments were done with approval of the Yale Institutional Animal Care and Use Committee.

Viruses, proteins, and cells
Influenza virus A/Puerto Rico/8/1934 H1N1 (PR8) was a kind gift from A. Iwasaki (Yale University, New Haven, CT). Clinical isolate influenza virus A/Michigan/45/2015 (H1N1) was used along with the following laboratory reassortant viruses: H5N1, A/Indonesia/05/2005 H5N1 low pathogenic H5 HA (with the polybasic cleavage site removed) with remaining influenza virus proteins from PR8; and H6N3, A/swine/Missouri/4296424/2006 H6N3 HA and NA with remaining influenza proteins from PR8.

Reassortant viruses were rescued as described previously (Martínez-Sobrido and García-Sastre, 2010). All viruses were propagated in 10-d-old specific pathogen–free eggs (Charles River) after inoculation with 100 PFUs of virus. Infected eggs were incubated at 37°C for 48 h before harvesting and clearance of allantoic fluid. Virus-containing fluid was aliquoted and stored at –80°C before infection. For purified viral stocks, allantoic fluid was spun at 125,000 g for 2 h over a 5% sucrose cushion. Pelleted virion particles were resuspended in PBS and stored at –80°C before vaccination.

Viral loads were measured by plaque assay on Madin–Darby canine kidney cells. Briefly, Madin–Darby canine kidney cells were plated in 6-well dishes at 8×10^5 cells/well and allowed to incubate overnight at 37°C and 5% CO_2. Samples were diluted in PBS and added to cells to allow viral absorption for 1 h at 37°C and 5% CO_2 with periodic shaking. Cells were then rinsed with PBS, and an agar overlay was added to allow the virus to infect in the presence of tosyl phenylalanyl chloromethyl ketone–treated trypsin. Plaques were visualized with crystal violet staining and counted.

All the recombinant HA and NA proteins used in ELISA and ELISPOT assays were kind gifts from F. Krammer (Icahn School of Medicine at Mount Sinai, New York, NY) and were generated and purified as previously described (Margine et al., 2013).

Infection and treatment
Mice were given i.n. administration of 8 PFUs of influenza virus A/PR8/34 (PR8) in 30 µl of PBS. Prior to i.n. infections, the mice were anesthetized by ketamine hydrochloride and xylazine (Phoenix Scientific) in 200 µl of PBS via i.p. injections. For the sequential vaccination strategy, mice were primed with 2.5 µg per mouse of the A/Michigan/45/2015 (H1N1) through intramuscular vaccination, followed 6 wk later by H5N1 vaccination intramuscularly. All the animals received a second boost on day 84 with H6N3. The influenza virus strains used in the sequential vaccination experiments were approved for usage by the Icahn School of Medicine at Mount Sinai Biosafety Committee.

Flow cytometry, cell sorting, and antibodies for surface and intracellular staining
Staining of transcription factors was performed after permeabilization with the FoxP3 Fixation and Permeabilization Kit (eBioscience). For intracellular cytokine staining, cells were stimulated with PMA (50 ng/ml) and ionomycin (1 µg/ml) in 96-well U-bottom plates in complete media for 4–5 h, and brefeldin A (BD Biosciences) was added for the last 3–4 h. Intracellular staining was performed using the BD ICS kit as per the manufacturer's instructions with overnight incubation (4°C) of permeabilized cells with transcription factor–specific antibodies. Antibodies are listed in Table S3. Recombinant HA probe for B cells was generated as previously described (Angeletti et al., 2017). The HA I-A(b) tetramer (PR8 HA 91–107 RSWSYIVETPNSENGIC; Miller et al., 2015) and the NP I-A(b) tetramer (NP 311–325 QVYSLIRPNENPAHK; Botta et al., 2017) were produced by the National Institutes of Health Tetramer Core Facility. Flow cytometry data were acquired on a BD LSRII with

FACSDiva software and were analyzed with FlowJo software (Tree Star).

Isolation of lymphocytes from tissues

mLNs were homogenized with a cell strainer. Lymphocytes were then washed and counted.

Confocal imaging

mLNs were prepared by overnight fixation at 4°C with periodate-lysine-paraformaldehyde buffer (50 mM phosphate buffer, 0.1 M L-lysine [Sigma-Aldrich], 1% paraformaldehyde [Sigma-Aldrich], and 0.2% sodium M-periodate [Sigma-Aldrich]). The fixed LNs were frozen in 100% optimum cutting temperature compound (VWR) in cryomolds and stored at –80°C. The frozen tissues were cut into 8-µm sections using a Cryostat Microtome (Leica) and processed as previously described (Joshi et al., 2015). In short, sections were incubated in ice-cold acetone for 15–20 min at –20°C and then washed 3 × 5 min with PBS. Sections were permeabilized and blocked in Immunomix (0.2% BSA [Sigma-Aldrich], 0.3% Triton X-100 [Sigma-Aldrich], and 10% rat serum [StemCell] in PBS). The sections were stained with antibodies (Table S3) diluted in Immunomix. Images were acquired on a Leica TCS SP5 Spectral Confocal Microscope with the objective at 40× magnification. ImageJ was used to quantify the size of GCs.

ELISA

ELISAs were performed as described previously (Nachbagauer et al., 2017). Specifically, 96-well high-binding, flat-bottomed plates were coated with 50 µl/well of recombinant HA protein at a concentration of 2 µg/ml in coating buffer (50 mM sodium carbonate and 50 mM sodium hydrogen carbonate, pH 9.4) and were incubated overnight at 4°C. The coating buffer was removed, and plates were incubated for 1 h at room temperature with 220 µl of blocking solution (3% goat serum, 0.5% Tween-20, and 3% milk powder in PBS). Serum was serially diluted threefold in blocking solution with a starting dilution of 1:50, and plates were incubated for 2 h at room temperature. Plates were then washed three times with PBS with 0.5% Tween-20 (PBS-T) followed by adding 50 µl of isotype-specific secondary antibody diluted in blocking solution to each well (IgG [ab97265], IgG1 [ab97240], and IgG2c [ab97255]; Abcam). After 1 h of incubation at room temperature, plates were washed four times with PBS-T. Plates were developed with 100 µl of SigmaFast OPD (Sigma-Aldrich), and the development was stopped after 10 min by adding 50 µl of 3 M HCl. Plates were then read at a wavelength of 490 nm with a Synergy H1 hybrid multimode microplate reader (BioTek). Background was determined as the average of blank wells plus three times the standard deviation between those wells. Area under the curve was measured after fitting a regression curve using the formula [Agonist] vs. response – variable slope (four parameters) and using the previously determined background value or 0.07, whichever was higher. To measure affinity by ELISA, a 10-min, 7 M urea wash was introduced after incubating serum samples with the HA substrate. Percentage of IgG binding after urea wash was determined by dividing the IgG bound to HA treated by 7 M urea by untreated IgG bound.

Total IgG were measured using Mouse IgG ELISA kit (Innovative Research) following manufacturer's instructions.

ELISPOT for HA-specific Igs

MultiScreen HTS plates (Millipore) were coated with 50 µl/well of recombinant HA protein at a concentration of 2 µg/ml in PBS overnight at 4°C. The coating solution was removed, and plates were washed six times with PBS-T followed by incubation with 200 µl of complete medium (10% fetal bovine serum and 1% L-glutamine, penicillin, and streptomycin in RPMI [Life Technologies]) for 2 h at 37°C. Subsequently, bone marrow cells from mice infected with the PR8 influenza virus were isolated and plated (3 × 10⁶ cells/well) in duplicate in complete medium for 4–5 h at 37°C. Plates were then washed six times with PBS-T followed by addition of secondary antibody (50 µl) in blocking solution (0.5% BSA in PBS; anti-IgG–alkaline phosphatase; Southern Biotech [1030–04]) to each well, then incubated overnight at 4°C. The plates were washed three times with PBS-T and three times with PBS. Spots were developed with Vector Blue (Vector Laboratories) and quantified using an ImmunoSpot analyzer (Cellular Technology Limited).

ANA detection

Serum dilutions of 1:20 and 1:5 in PBS were used. ANA staining was performed using commercial HEp-2 slides (Antibodies Inc., 15-123) following the manufacturer's instructions, with degree of staining graded in a blinded manner (Peng and Craft, 2020).

BCR repertoire library preparation and data analysis

Lymphocytes from mLNs were isolated as described above and enriched for B cells by positive selection using magnetic beads (StemCell). GC B cells from infected animals were sorted as B220⁺, IgD^low, GL7⁺, CD95⁺ cells, and naive follicular B cells from uninfected animals were sorted as B220⁺, IgM⁺, CD23⁺ CD21⁻ cells. Following FACS sorting, cells of both types were pelleted, and RNA was isolated with the use of the RNeasy Plus Micro Kit (Qiagen). High-quality RNA with an RNA integrity number >9 was subsequently used to prepare BCR libraries with the NEBNext Immune Sequencing Kit (mouse; New England Biolabs) following the manufacturer's instructions. Specifically, ~50–100 ng of RNA was reverse transcribed into cDNA with the addition of a unique molecular identifier (UMI) and an adaptor sequence followed by purification of the nascent cDNA using streptavidin magnetic beads. A PCR reaction was conducted to amplify the VDJ region of the heavy chain and incorporate the index barcode followed by a subsequent cleanup of the PCR products with AMPure XP beads (Beckman Coulter). Quantitative PCR analysis was performed to determine the optimal number of cycles for the second PCR amplification of each sample. This second PCR was then performed with the addition of a P5 adaptor to the Ig constant region and a sample-indexed P7 adaptor to the universal adaptor end. Final PCR products were purified again using AMPure XP beads and quantified through automated electrophoresis (Tapestation; Agilent). Equal amounts of each sample (6 µg) were pooled and followed by high-throughput 325 + 275 base pair paired-end

sequencing with 30% PhiX spike-in on the Illumina MiSeq platform according to the manufacturer's guidelines.

Processing of BCR repertoires was performed using tools from the Immcantation framework (http://immcantation.org). The following preprocessing steps were performed using pRESTO v0.5.10 tools (Vander Heiden et al., 2014). Reads with a mean Phred score <20 were removed. Constant region (>0.8 identity) and template switch primers (>0.5 identity) were identified, while those sequences without a match were excluded. Primer sequences for pRESTO were TS-Shift0 TACGGG, TS-Shift1 ATACGGG, TS-Shift2 TCTACGGG, TS-shift3 CGATACGGG, and TS-shift4 GATCTACGGG. UMI sequences were identified from the first 17 nucleotides preceding the template switch site. A consensus sequence was constructed for forward and reverse reads for each UMI group and was aligned with a minimum overlap of eight nucleotides and with a mismatch identity <0.3 to assemble VDJ sequences. To reconstruct full-length VDJ sequences, sequence pairs failing alignment were aligned against the ImMunoGeneTics (IMGT) mouse immunoglogbulin V_H genes reference database (IMGT/GENE-DB v3.1.19; retrieved June 21, 2018; mismatch identity <0.5; E-value threshold <1 × 10–5.6). Duplicate VDJ sequences were removed. IgBLAST v1.7.0 was used for germline assignments (Ye et al., 2013). Nonfunctional VDJ sequences were removed. Clonal clusters were assigned using Change-O v0.3.4, an approach described previously, and a junction threshold of 0.084 was used (Gupta et al., 2015). Germline sequences were then reconstructed for each clonal cluster (V_H) with D segment and N/P regions masked (replaced with Ns) using the CreateGermlines.py function within Change-O v0.3.4. Mutations and the mutabilities of potential motifs were quantified using ShazaM v0.1.8 in R v3.4.2 relative to germline sequences. Diversity analysis was performed using tools from Alakazam v0.2.11 and assessed using the generalized Hill index involving downsampling to the number of VDJ sequences from the sample with the fewest sequences and 2,000 bootstrap replicates (Hill, 1973). Selection strengths were quantified using the BASELINe implementation for complementarity determining region and framework region (Yaari et al., 2012). Aggregate posterior distribution functions for each genotype were determined via convolution of posterior distribution functions from each sample of a given genotype.

The BCR sequencing data reported in this paper are tabulated in the online supplemental material and archived at NCBI BioProject (accession no. PRJNA673160).

RNA-seq library preparation and data analysis

Total RNA was purified with the use of a QIAzol and RNeasy Plus Micro kit (Qiagen). Purified total RNA was submitted to the Yale Center for Genomic Analysis, where it was subjected to isolation of mRNA and library preparation. Libraries were pooled, six samples per lane, and were sequenced on an Illumina HiSeq 2500 (75 base pair paired-end reads), followed by alignment with STAR software (Anders et al., 2013). A "count-based" differential expression protocol was adapted for this analysis (Anders et al., 2013). Mappable reads were counted with the feature Count and imported into R software for analysis of differential expression with DESeq2 software. A multi-factor design was used to analyze the two conditions ($Bcl6^{f/f}$ Foxp3-Cre and $Bcl6^{f/f}$) and account for pairwise groupings of the six samples. For the generation of the volcano plot, genes with average counts >1 were chosen for visualization. The RNA sequencing data are archived in the NCBI GEO database (accession no. GSE161788).

Statistical analysis

Results represent the mean ± SEM unless indicated otherwise. Statistical significance was determined by the paired or unpaired Student's t test. Statistical analyses were performed using Prism GraphPad software v7.0 (*, $P < 0.05$; **, $P < 0.01$; ***, $P < 0.001$) except in Fig. 4 C (a two-tailed Wilcoxon test was used with a significance threshold of *, $P < 0.1$; **, $P < 0.05$). Principal component analysis was performed using the pca function in R. Pearson correlation coefficients were computed using the corr.test function in base R.

Online supplemental material

Fig. S1 shows the kinetics of CD4+ Tfr cells, Tfh cells, GC B cells, and HA-specific GC B cells following influenza virus infection and characterization of Tfr cell–deficient animals. Fig. S2 illustrates that $Bcl6^{f/f}$ Foxp3-Cre animals have reduced HA-specific GC B cells and antibody response as compared with Foxp3-Cre littermate controls. Fig. S3 reveals that Tfr cell–deficient animals show weakly positive ANA staining following influenza virus infection. Fig. S4 shows that mice lacking CD4+ Tfr cells mount similar Tfh cell responses as compared with control mice at 8 and 38 d following influenza virus infection. Fig. S5 demonstrates that many mLN Igh repertoire features are consistent between wild-type and mice lacking CD4+ Tfr, including clonality, selection pressure, isotype usage, and somatic hypermutation. Table S1 lists the differentially expressed genes in Tfh cells between $Bcl6^{f/f}$ Foxp3-Cre and $Bcl6^{f/f}$ mice with adjusted P value <0.05. Table S2 is a summary of sequencing reads and reconstructed Igh VDJ sequences from naive and infected $Bcl6^{f/f}$ and $Bcl6^{f/f}$ Foxp3-Cre mice. Table S3 shows antibodies used for flow cytometry and microscopy.

Acknowledgments

References

Anders, S., D.J. McCarthy, Y. Chen, M. Okoniewski, G.K. Smyth, W. Huber, and M.D. Robinson. 2013. Count-based differential expression analysis of RNA sequencing data using R and Bioconductor. *Nat. Protoc.* 8: 1765–1786. https://doi.org/10.1038/nprot.2013.099

Andrews, S.F., Y. Huang, K. Kaur, L.I. Popova, I.Y. Ho, N.T. Pauli, C.J. Henry Dunand, W.M. Taylor, S. Lim, M. Huang, et al. 2015. Immune history profoundly affects broadly protective B cell responses to influenza. *Sci. Transl. Med.* 7:316ra192. https://doi.org/10.1126/scitranslmed.aad0522

Angeletti, D., J.S. Gibbs, M. Angel, I. Kosik, H.D. Hickman, G.M. Frank, S.R. Das, A.K. Wheatley, M. Prabhakaran, D.J. Leggat, et al. 2017. Defining B cell immunodominance to viruses. *Nat. Immunol.* 18:456–463. https://doi.org/10.1038/ni.3680

Botta, D., M.J. Fuller, T.T. Marquez-Lago, H. Bachus, J.E. Bradley, A.S. Weinmann, A.J. Zajac, T.D. Randall, F.E. Lund, B. León, and A. Ballesteros-Tato. 2017. Dynamic regulation of T follicular regulatory cell responses by interleukin 2 during influenza infection. *Nat. Immunol.* 18: 1249–1260. https://doi.org/10.1038/ni.3837

Böttcher-Friebertshäuser, E., C. Freuer, F. Sielaff, S. Schmidt, M. Eickmann, J. Uhlendorff, T. Steinmetzer, H.-D. Klenk, and W. Garten. 2010. Cleavage of influenza virus hemagglutinin by airway proteases TMPRSS2 and HAT differs in subcellular localization and susceptibility to protease inhibitors. *J. Virol.* 84:5605–5614. https://doi.org/10.1128/JVI.00140-10

Chen, Y.Q., T.J. Wohlbold, N.Y. Zheng, M. Huang, Y. Huang, K.E. Neu, J. Lee, H. Wan, K.T. Rojas, E. Kirkpatrick, et al. 2018. Influenza Infection in Humans Induces Broadly Cross-Reactive and Protective Neuraminidase-Reactive Antibodies. *Cell.* 173:417–429.e10. https://doi.org/10.1016/j.cell.2018.03.030

Choi, A., B. Bouzya, K.D. Cortés Franco, D. Stadlbauer, A. Rajabhathor, R.N. Rouxel, R. Mainil, M. Van der Wielen, P. Palese, A. García-Sastre, et al. 2019. Chimeric Hemagglutinin-Based Influenza Virus Vaccines Induce Protective Stalk-Specific Humoral Immunity and Cellular Responses in Mice. *Immunohorizons.* 3:133–148. https://doi.org/10.4049/immunohorizons.1900022

Chung, Y., S. Tanaka, F. Chu, R.I. Nurieva, G.J. Martinez, S. Rawal, Y.-H. Wang, H. Lim, J.M. Reynolds, X.-H. Zhou, et al. 2011. Follicular regulatory T cells expressing Foxp3 and Bcl-6 suppress germinal center reactions. *Nat. Med.* 17:983–988. https://doi.org/10.1038/nm.2426

Clement, R.L., J. Daccache, M.T. Mohammed, A. Diallo, B.R. Blazar, V.K. Kuchroo, S.B. Lovitch, A.H. Sharpe, and P.T. Sage. 2019. Follicular regulatory T cells control humoral and allergic immunity by restraining early B cell responses. *Nat. Immunol.* 20:1360–1371. https://doi.org/10.1038/s41590-019-0472-4

Crotty, S. 2011. Follicular helper CD4 T cells (TFH). *Annu. Rev. Immunol.* 29: 621–663. https://doi.org/10.1146/annurev-immunol-031210-101400

De Silva, N.S., and U. Klein. 2015. Dynamics of B cells in germinal centres. *Nat. Rev. Immunol.* 15:137–148. https://doi.org/10.1038/nri3804

Dominguez-Sola, D., G.D. Victora, C.Y. Ying, R.T. Phan, M. Saito, M.C. Nussenzweig, and R. Dalla-Favera. 2012. The proto-oncogene MYC is required for selection in the germinal center and cyclic reentry. *Nat. Immunol.* 13:1083–1091. https://doi.org/10.1038/ni.2428

Eisen, H.N. 2014. Affinity enhancement of antibodies: how low-affinity antibodies produced early in immune responses are followed by high-affinity antibodies later and in memory B-cell responses. *Cancer Immunol. Res.* 2: 381–392. https://doi.org/10.1158/2326-6066.CIR-14-0029

Ersching, J., A. Efeyan, L. Mesin, J.T. Jacobsen, G. Pasqual, B.C. Grabiner, D. Dominguez-Sola, D.M. Sabatini, G.D. Victora, J.T. Jacobsen, et al. 2017. Germinal Center Selection and Affinity Maturation Require Dynamic Regulation of mTORC1 Kinase. *Immunity.* 46:1045–1058.e6. https://doi.org/10.1016/j.immuni.2017.06.005

Fu, W., X. Liu, X. Lin, H. Feng, L. Sun, S. Li, H. Chen, H. Tang, L. Lu, W. Jin, and C. Dong. 2018. Deficiency in T follicular regulatory cells promotes autoimmunity. *J. Exp. Med.* 215:815–825. https://doi.org/10.1084/jem.20170901

Gitlin, A.D., Z. Shulman, and M.C. Nussenzweig. 2014. Clonal selection in the germinal centre by regulated proliferation and hypermutation. *Nature.* 509:637–640. https://doi.org/10.1038/nature13300

Gupta, N.T., J.A. Vander Heiden, M. Uduman, D. Gadala-Maria, G. Yaari, and S.H. Kleinstein. 2015. Change-O: a toolkit for analyzing large-scale B cell immunoglobulin repertoire sequencing data. *Bioinformatics.* 31: 3356–3358. https://doi.org/10.1093/bioinformatics/btv359

Hill, M.O. 1973. Diversity and Evenness: A Unifying Notation and Its Consequences. *Ecology.* 54:427–432. https://doi.org/10.2307/1934352

Jacobsen, H., M. Rajendran, A. Choi, H. Sjursen, K.A. Brokstad, R.J. Cox, P. Palese, F. Krammer, and R. Nachbagauer. 2017. Influenza Virus Hemagglutinin Stalk-Specific Antibodies in Human Serum are a Surrogate Marker for *In Vivo* Protection in a Serum Transfer Mouse Challenge Model. *MBio.* 8:e01463-17. https://doi.org/10.1128/mBio.01463-17

Josefowicz, S.Z., L.-F. Lu, and A.Y. Rudensky. 2012. Regulatory T cells: mechanisms of differentiation and function. *Annu. Rev. Immunol.* 30: 531–564. https://doi.org/10.1146/annurev.immunol.25.022106.141623

Joshi, N.S., E.H. Akama-Garren, Y. Lu, D.-Y. Lee, G.P. Chang, A. Li, M. DuPage, T. Tammela, N.R. Kerper, A.F. Farago, et al. 2015. Regulatory T Cells in Tumor-Associated Tertiary Lymphoid Structures Suppress Anti-tumor T Cell Responses. *Immunity.* 43:579–590. https://doi.org/10.1016/j.immuni.2015.08.006

Kalia, V., L.A. Penny, Y. Yuzefpolskiy, F.M. Baumann, and S. Sarkar. 2015. Quiescence of Memory CD8(+) T Cells Is Mediated by Regulatory T Cells through Inhibitory Receptor CTLA-4. *Immunity.* 42:1116–1129. https://doi.org/10.1016/j.immuni.2015.05.023

Kuraoka, M., A.G. Schmidt, T. Nojima, F. Feng, A. Watanabe, D. Kitamura, S.C. Harrison, T.B. Kepler, and G. Kelsoe. 2016. Complex Antigens Drive Permissive Clonal Selection in Germinal Centers. *Immunity.* 44:542–552. https://doi.org/10.1016/j.immuni.2016.02.010

Laidlaw, B.J., W. Cui, R.A. Amezquita, S.M. Gray, T. Guan, Y. Lu, Y. Kobayashi, R.A. Flavell, S.H. Kleinstein, J. Craft, and S.M. Kaech. 2015. Production of IL-10 by CD4(+) regulatory T cells during the resolution of infection promotes the maturation of memory CD8(+) T cells. *Nat. Immunol.* 16:871–879. https://doi.org/10.1038/ni.3224

Laidlaw, B.J., J.E. Craft, and S.M. Kaech. 2016. The multifaceted role of CD4(+) T cells in CD8(+) T cell memory. *Nat. Rev. Immunol.* 16:102–111. https://doi.org/10.1038/nri.2015.10

Laidlaw, B.J., Y. Lu, R.A. Amezquita, J.S. Weinstein, J.A. Vander Heiden, N.T. Gupta, S.H. Kleinstein, S.M. Kaech, and J. Craft. 2017. Interleukin-10 from CD4+ follicular regulatory T cells promotes the germinal center response. *Sci. Immunol.* 2:eaan4767. https://doi.org/10.1126/sciimmunol.aan4767

Linterman, M.A., W. Pierson, S.K. Lee, A. Kallies, S. Kawamoto, T.F. Rayner, M. Srivastava, D.P. Divekar, L. Beaton, J.J. Hogan, et al. 2011. Foxp3+ follicular regulatory T cells control the germinal center response. *Nat. Med.* 17:975–982. https://doi.org/10.1038/nm.2425

Margine, I., P. Palese, and F. Krammer. 2013. Expression of functional recombinant hemagglutinin and neuraminidase proteins from the novel H7N9 influenza virus using the baculovirus expression system. *J. Vis. Exp.* https://doi.org/10.3791/51112

Marshall, H.D., A. Chandele, Y.W. Jung, H. Meng, A.C. Poholek, I.A. Parish, R. Rutishauser, W. Cui, S.H. Kleinstein, J. Craft, and S.M. Kaech. 2011. Differential expression of Ly6C and T-bet distinguish effector and memory Th1 CD4(+) cell properties during viral infection. *Immunity.* 35: 633–646. https://doi.org/10.1016/j.immuni.2011.08.016

Martínez-Sobrido, L., and A. García-Sastre. 2010. Generation of recombinant influenza virus from plasmid DNA. *J. Vis. Exp.* https://doi.org/10.3791/2057

Miller, M.A., A.P.V. Ganesan, N. Luckashenak, M. Mendonca, and L.C. Eisenlohr. 2015. Endogenous antigen processing drives the primary CD4+ T cell response to influenza. *Nat. Med.* 21:1216–1222. https://doi.org/10.1038/nm.3958

Nachbagauer, R., and P. Palese. 2020. Is a Universal Influenza Virus Vaccine Possible? *Annu. Rev. Med.* https://doi.org/10.1146/annurev-med-120617-041310

Nachbagauer, R., T.J. Wohlbold, A. Hirsh, R. Hai, H. Sjursen, P. Palese, R.J. Cox, and F. Krammer. 2014. Induction of broadly reactive anti-hemagglutinin

stalk antibodies by an H5N1 vaccine in humans. *J. Virol.* 88:13260–13268. https://doi.org/10.1128/JVI.02133-14

Nachbagauer, R., D. Kinzler, A. Choi, A. Hirsh, E. Beaulieu, N. Lecrenier, B.L. Innis, P. Palese, C.P. Mallett, and F. Krammer. 2016. A chimeric haemagglutinin-based influenza split virion vaccine adjuvanted with AS03 induces protective stalk-reactive antibodies in mice. *NPJ Vaccines.* 1:16015. https://doi.org/10.1038/npjvaccines.2016.15

Nachbagauer, R., A. Choi, A. Hirsh, I. Margine, S. Iida, A. Barrera, M. Ferres, R.A. Albrecht, A. García-Sastre, N.M. Bouvier, et al. 2017. Defining the antibody cross-reactome directed against the influenza virus surface glycoproteins. *Nat. Immunol.* 18:464–473. https://doi.org/10.1038/ni.3684

Nutt, S.L., P.D. Hodgkin, D.M. Tarlinton, and L.M. Corcoran. 2015. The generation of antibody-secreting plasma cells. *Nat. Rev. Immunol.* 15:160–171. https://doi.org/10.1038/nri3795

Pace, L., A. Tempez, C. Arnold-Schrauf, F. Lemaitre, P. Bousso, L. Fetler, T. Sparwasser, and S. Amigorena. 2012. Regulatory T cells increase the avidity of primary CD8+ T cell responses and promote memory. *Science.* 338:532–536. https://doi.org/10.1126/science.1227049

Peng, S., and J. Craft. 2020. Antinuclear antibodies. *In* Firestein and Kelley's Textbook of Rheumatology. 11th edition. G.S. Firestein, R.C. Rudd, S.E. Gabriel, I.A. Mclness, J.R. O'Dell, and G. Koretsky, editors. Elsevier, Philadelphia. 875–889.

Roers, A., L. Siewe, E. Strittmatter, M. Deckert, D. Schlüter, W. Stenzel, A.D. Gruber, T. Krieg, K. Rajewsky, and W. Müller. 2004. T cell-specific inactivation of the interleukin 10 gene in mice results in enhanced T cell responses but normal innate responses to lipopolysaccharide or skin irritation. *J. Exp. Med.* 200:1289–1297. https://doi.org/10.1084/jem.20041789

Sage, P.T., A.M. Paterson, S.B. Lovitch, and A.H. Sharpe. 2014. The co-inhibitory receptor CTLA-4 controls B cell responses by modulating T follicular helper, T follicular regulatory, and T regulatory cells. *Immunity.* 41:1026–1039. https://doi.org/10.1016/j.immuni.2014.12.005

Sage, P.T., N. Ron-Harel, V.R. Juneja, D.R. Sen, S. Maleri, W. Sungnak, V.K. Kuchroo, W.N. Haining, N. Chevrier, M. Haigis, and A.H. Sharpe. 2016. Suppression by T$_{FR}$ cells leads to durable and selective inhibition of B cell effector function. *Nat. Immunol.* 17:1436–1446. https://doi.org/10.1038/ni.3578

Schmidt-Supprian, M., and K. Rajewsky. 2007. Vagaries of conditional gene targeting. *Nat. Immunol.* 8:665–668. https://doi.org/10.1038/ni0707-665

Shulman, Z., A.D. Gitlin, J.S. Weinstein, B. Lainez, E. Esplugues, R.A. Flavell, J.E. Craft, and M.C. Nussenzweig. 2014. Dynamic signaling by T follicular helper cells during germinal center B cell selection. *Science.* 345:1058–1062. https://doi.org/10.1126/science.1257861

Tas, J.M.J., L. Mesin, G. Pasqual, S. Targ, J.T. Jacobsen, Y.M. Mano, C.S. Chen, J.-C. Weill, C.-A. Reynaud, E.P. Browne, et al. 2016. Visualizing antibody affinity maturation in germinal centers. *Science.* 351:1048–1054. https://doi.org/10.1126/science.aad3439

Vander Heiden, J.A., G. Yaari, M. Uduman, J.N.H. Stern, K.C. O'Connor, D.A. Hafler, F. Vigneault, and S.H. Kleinstein. 2014. pRESTO: a toolkit for processing high-throughput sequencing raw reads of lymphocyte receptor repertoires. *Bioinformatics.* 30:1930–1932. https://doi.org/10.1093/bioinformatics/btu138

Victora, G.D., and M.C. Nussenzweig. 2012. Germinal centers. *Annu. Rev. Immunol.* 30:429–457. https://doi.org/10.1146/annurev-immunol-020711-075032

Victora, G.D., T.A. Schwickert, D.R. Fooksman, A.O. Kamphorst, M. Meyer-Hermann, M.L. Dustin, and M.C. Nussenzweig. 2010. Germinal center dynamics revealed by multiphoton microscopy with a photoactivatable fluorescent reporter. *Cell.* 143:592–605. https://doi.org/10.1016/j.cell.2010.10.032

Whittle, J.R.R., A.K. Wheatley, L. Wu, D. Lingwood, M. Kanekiyo, S.S. Ma, S.R. Narpala, H.M. Yassine, G.M. Frank, J.W. Yewdell, et al. 2014. Flow cytometry reveals that H5N1 vaccination elicits cross-reactive stem-directed antibodies from multiple Ig heavy-chain lineages. *J. Virol.* 88:4047–4057. https://doi.org/10.1128/JVI.03422-13

Wing, J.B., W. Ise, T. Kurosaki, and S. Sakaguchi. 2014. Regulatory T cells control antigen-specific expansion of Tfh cell number and humoral immune responses via the coreceptor CTLA-4. *Immunity.* 41:1013–1025. https://doi.org/10.1016/j.immuni.2014.12.006

Wollenberg, I., A. Agua-Doce, A. Hernández, C. Almeida, V.G. Oliveira, J. Faro, and L. Graca. 2011. Regulation of the germinal center reaction by Foxp3+ follicular regulatory T cells. *J. Immunol.* 187:4553–4560. https://doi.org/10.4049/jimmunol.1101328

Yaari, G., M. Uduman, and S.H. Kleinstein. 2012. Quantifying selection in high-throughput Immunoglobulin sequencing data sets. *Nucleic Acids Res.* 40:e134. https://doi.org/10.1093/nar/gks457

Ye, J., N. Ma, T.L. Madden, and J.M. Ostell. 2013. IgBLAST: an immunoglobulin variable domain sequence analysis tool. *Nucleic Acids Res.* 41(W1, Web Server issue):W34-40. https://doi.org/10.1093/nar/gkt382
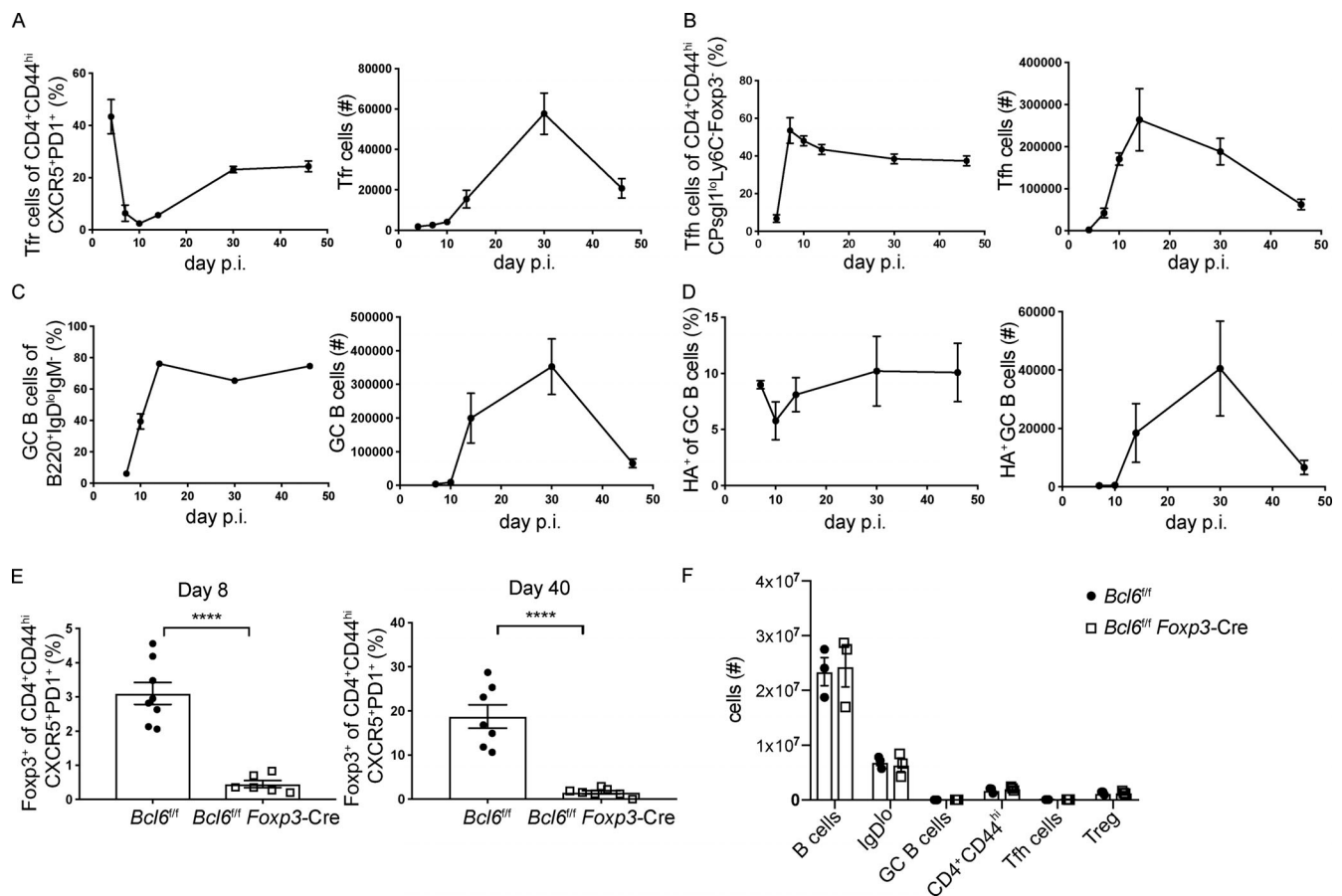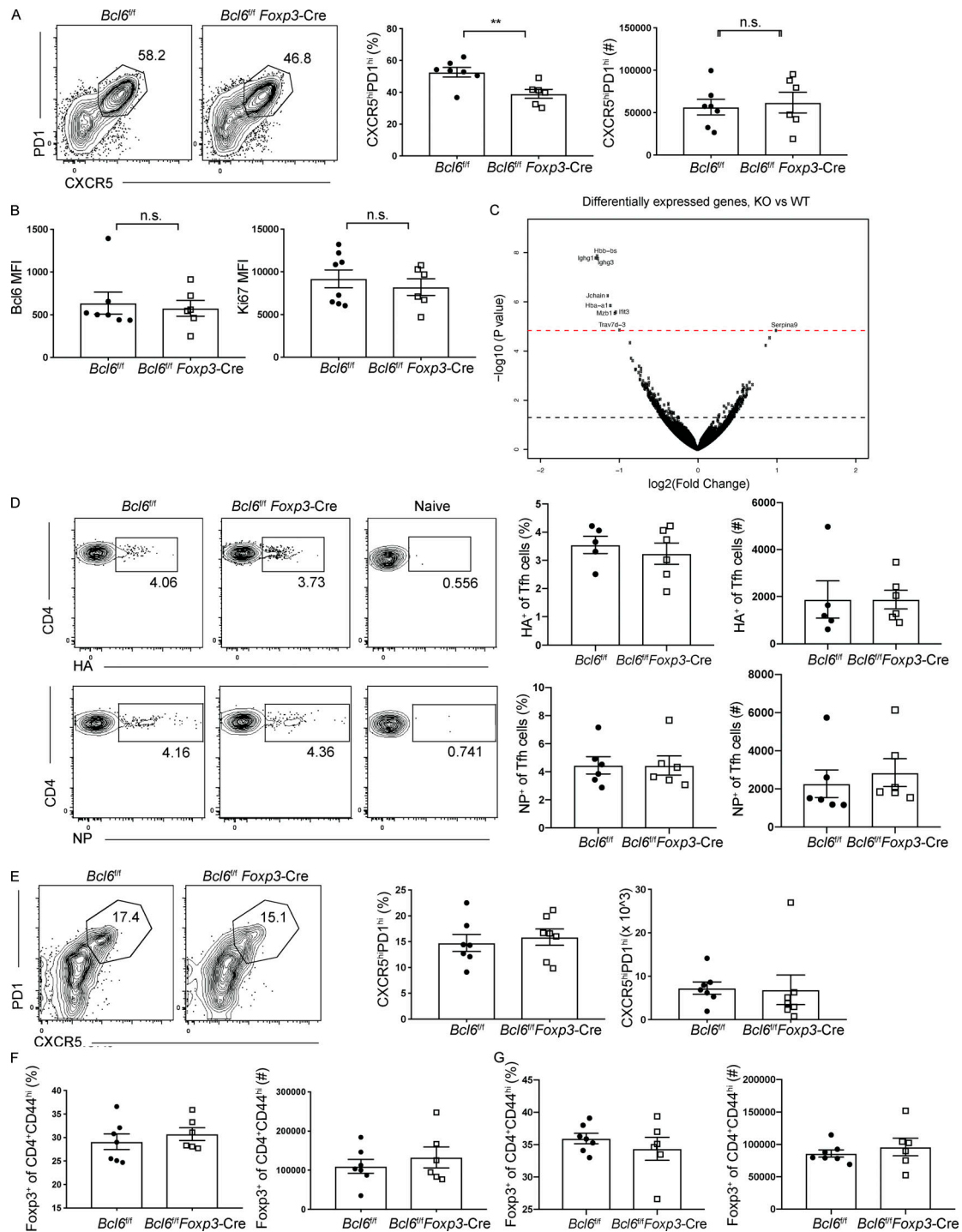
Figure S1. **The kinetics of follicular regulatory CD4+ T cells, Tfh cells, GC B cells, and HA-specific GC B cells following influenza virus infection and characterization of Tfr cell–deficient animals. (A)** Frequency and number of Tfr cells defined as CD4+CD44hiLy6C−PSGL1lowCXCR5hiPD1hiFoxp3+. **(B)** Frequency and number of Tfh cells defined as CD4+CD44hiFoxp3−Ly6C−PSGL1lowCXCR5hiPD1hi. **(C)** Frequency and number of GC B cells defined as B220+IgDloGL7+CD38−. **(D)** Frequency and number of HA-specific GC B cells defined as B220+IgM−IgDloGL7+CD38−HA+. **(E)** Bcl6f/f Foxp3-Cre mice have a lack of Tfr cells. Frequencies of Tfr cells at days 8 and 40 p.i. in Tfr cell–sufficient (Bcl6f/f) and Tfr cell–deficient (Bcl6f/f Foxp3-Cre) mice. **(F)** Analyses of the number of B cells, activated B cells, GC B cells, activated CD4+ T cells, Tfh cells, and Treg cells in the spleen of naive Bcl6f/f and Bcl6f/f Foxp3-Cre animals. Statistical analyses were performed using the unpaired two-tailed Student's t test (****, P < 0.0001). Data for A–D are from one experiment representative of two experiments with three to six mice per time point after influenza virus infection. Data for E are from one experiment representative of three experiments with six to eight mice per group. Data for F are from one experiment representative of two experiments with three or four mice per group.
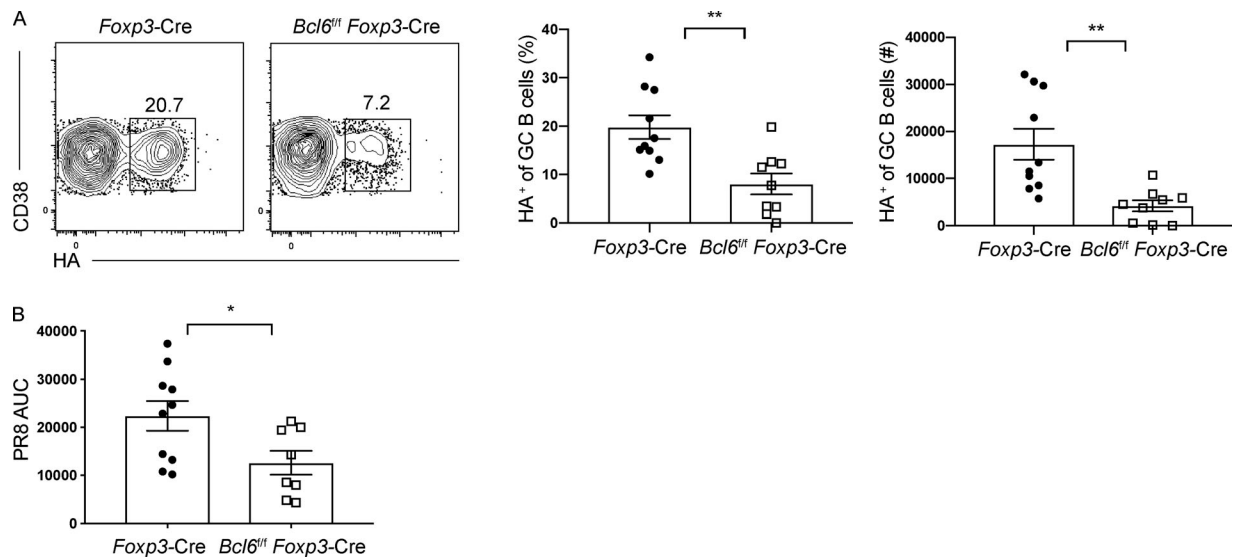
Figure S2. **Bcl6^f/f Foxp3-Cre animals have reduced HA-specific GC B cells and antibody response compared with Foxp3-Cre littermate controls.**
(A) Analysis of the GC B cell responses in *Foxp3*-Cre and *Bcl6*^f/f *Foxp3*-Cre mice at day 38 following influenza virus infection. Left: Representative plots of the HA^+ GC B cell responses in *Foxp3*-Cre and *Bcl6*^f/f *Foxp3*-Cre mice at day 38 p.i. Right: Frequency and number of cells as indicated by the gates shown on the left. **(B)** ELISA analysis of serum influenza-specific antibody titers in *Bcl6*^f/f *Foxp3*-Cre and littermate wild-type *Foxp3*-Cre mice at day 38 p.i. Statistical analyses were performed using the unpaired two-tailed Student's *t* test (*, P < 0.05; **, P < 0.01). Data are pooled from two independent experiments with four to six mice per group. AUC, area under the curve.

Figure S3.   **Tfr cell–deficient animals show weakly positive ANA staining following influenza virus infection. (A–D)** Representative images of ANA staining from *Bcl6*^f/f^ and *Bcl6*^f/f^ *Foxp3*-Cre mice at 36 d following influenza virus infection, with a serum dilution of 1:20; positive control from a 6-mo MRL/*lpr* mouse, scale bar, 100 µm (A); naive 4-mo-old *Bcl6*^f/f^ and *Bcl6*^f/f^ *Foxp3*-Cre mice, with a serum dilution of 1:20 (B); *Bcl6*^f/f^ and *Bcl6*^f/f^ *Foxp3*-Cre mice at 36 d following influenza virus infection, with a serum dilution of 1:5 (C); naive 4-mo-old *Bcl6*^f/f^ and *Bcl6*^f/f^ *Foxp3*-Cre mice, with a serum dilution of 1:5 (D). **(E)** Blinded scoring of ANA staining for *Bcl6*^f/f^ and *Bcl6*^f/f^ *Foxp3*-Cre mice at 36 d following influenza virus infection. Negative control is serum from a naive 6-wk-old B6 animal, and positive control serum is from a lupus-prone 6-mo-old MRL/*lpr* mouse. Data are from one experiment representative of two independent experiments with five to seven mice per group. *, P < 0.05. Data from A–D are from three individual mice per condition from one experiment.

Figure S4. **Mice lacking follicular regulatory CD4⁺ T cells mount similar Tfh cell responses compared with control mice at 8 and 38 d following influenza virus infection. (A)** Left: Representative plots of the polyclonal CD4⁺ Tfh cell response in *Bcl6*^f/f *Foxp3*-Cre and *Bcl6*^f/f mice at day 8 p.i. CD4⁺CD44⁺Foxp3⁻PSGL1^low Ly6C⁻ cells were gated on CXCR5 and PD1 to define the Tfh cell population. Right: Quantification of the percentage and number of Tfh cells as shown in the left plots. **(B)** Mean fluorescence intensity (MFI) of Bcl6 (left) and Ki67 (right) intracellular staining in Tfh cells gated as described. **(C)** Volcano plot of differentially expressed genes from RNA-seq of CD4⁺ Tfh cells from *Bcl6*^f/f and *Bcl6*^f/f *Foxp3*-Cre mice at 8 d p.i. The red dashed line plotted indicates the level of Bonferroni-corrected P value <0.05. **(D)** Left: Representative plots of the HA-specific and NP-specific CD4⁺ Tfh cell response in *Bcl6*^f/f *Foxp3*-Cre, *Bcl6*^f/f and naive mice at day 8 p.i. Tfh cells were gated as described in A; T cells from naive mice were gated on CD4⁺ CD44^hi population. Right: Quantification of the percentage and number of HA-specific and NP-specific Tfh cells as shown in the left plots. **(E)** Left: Representative plots of the polyclonal CD4⁺ Tfh cell response in *Bcl6*^f/f *Foxp3*-Cre and *Bcl6*^f/f mice at day 38 p.i. Right: Quantification of the percentage and number of Tfh cells as shown in the left plots. **(F and G)** Quantification of the percentage and number of Treg cells in *Bcl6*^f/f *Foxp3*-Cre and *Bcl6*^f/f mice at day 8 p.i. and day 38 p.i., respectively. Statistical analyses were performed using the unpaired two-tailed Student's *t* test (**, P < 0.01). Data for A, B, and E–G are from one experiment representative of three experiments with five to eight mice per group. Data for C are from three independent experiments with three or four mice per group pooled for each sample. Data for D are from one experiment representative of two experiments with four to six mice per group. n.s., not significant.
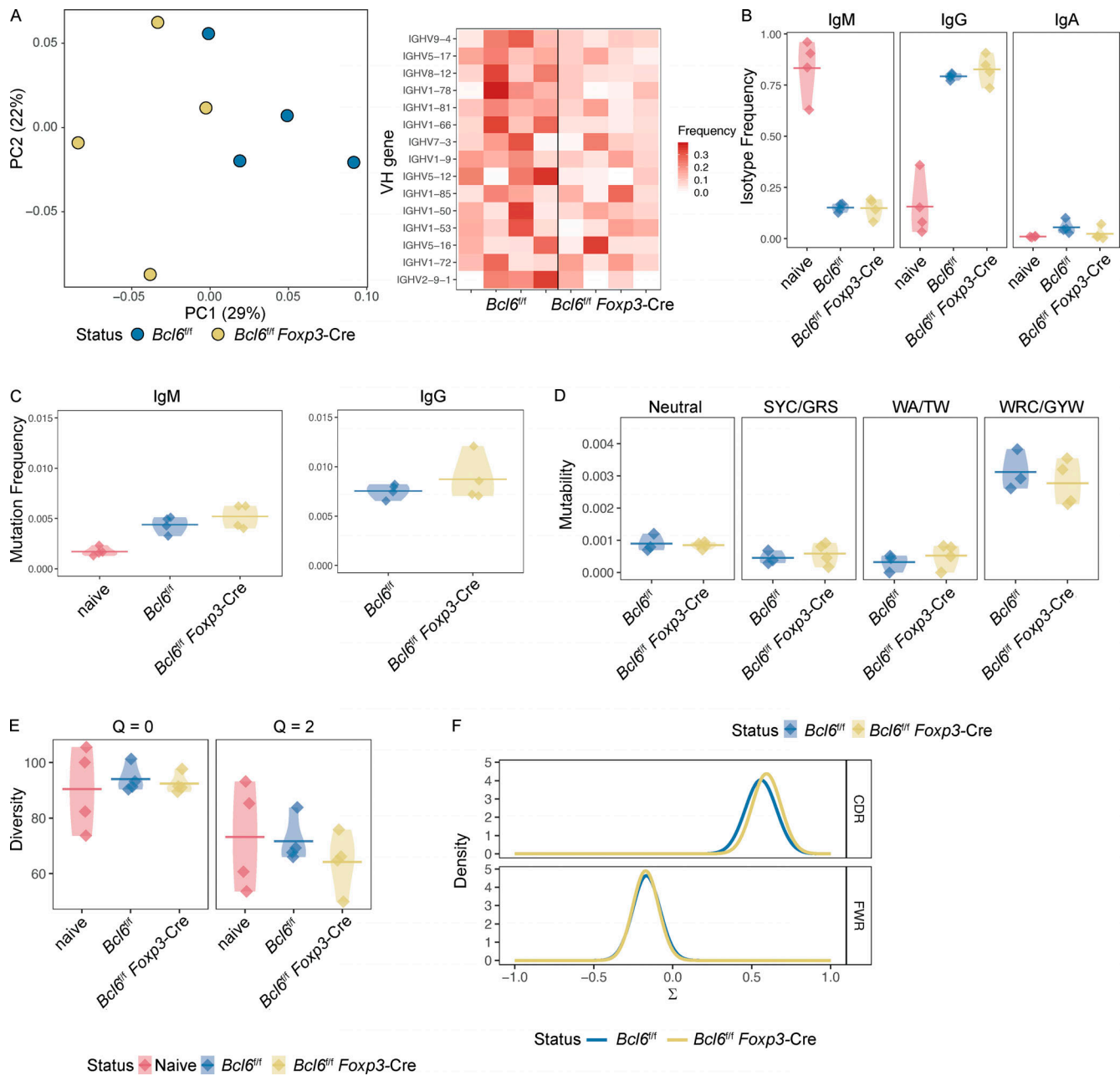
Figure S5. **Many mLN Igh repertoire features are consistent between wild-type and mice lacking follicular regulatory CD4+ T, including clonality, selection pressure, isotype usage, and somatic hypermutation. (A)** Left: Principal component analysis visualization of V_H gene usage frequency for *Igh* sequences associated with an IgG constant region. Right: Heatmaps showing V_H gene usage frequencies for the top 15 V_H genes based on maximal principal component 1 score from the principal component analysis of IgG-only sequences. **(B)** Overall isotype usage of IgM, IgG, and IgA. Horizontal bars indicate the mean isotype frequency. **(C)** Somatic hypermutation frequencies of the V_H gene region for IgG and IgM. Igh somatic hypermutation frequencies are computed relative to the best matched germline references from IMGT. Horizontal bars indicate the mean of the mutation frequency. **(D)** Mutability, the frequency at which 5-mer sequences with hot (WRC/GYW and WA/TW) or cold (SYC/GRS) spots are observed to be mutated, is plotted for each sample. Horizontal bars show the mean mutability frequency. **(E)** Clonal diversity at Hill diversity indices of Q = 0 (richness) and Q = 2 are plotted. Each point represents an estimated diversity score based on bootstrap realizations of the clonal abundance curve from each sample. Horizontal bars correspond to the mean diversity index across samples of a given genotype. **(F)** Baseline selection pressure analysis is shown as a density on the y axis and selection strength ($\mathring{a}$) on the x axis for both the complementarity determining region (CDR) and the framework region (FWR). For BCR repertoire analysis, data are from one experiment with four mice per group performed 15 d following PR8 influenza virus infection.

Three tables are posted online as separate files. Table S1 lists the differentially expressed genes in Tfh cells between *Bcl6*[f/f] *Foxp3*-Cre and *Bcl6*[f/f] mice with adjusted P value < 0.05. Table S2 is a summary of sequencing reads and reconstructed *Igh* VDJ sequences from naive and infected *Bcl6*[f/f] and *Bcl6*[f/f] *Foxp3*-Cre mice. Table S3 lists antibodies used for flow cytometry and microscopy.